# THE EFFECT OF SURFACTANT ON THE MORPHOLOGY OF METHANE/PROPANE CLATHRATE HYDRATE CRYSTALS

by

**JEFFRY YOSLIM**

B.A.Sc., University of British Columbia, 2006

A THESIS SUBMITTED IN PARTIAL FULFILLMENT OF
THE REQUIREMENTS FOR THE DEGREE OF

MASTER OF APPLIED SCIENCE
in
THE FACULTY OF GRADUATE STUDIES

(Chemical and Biological Engineering)

THE UNIVERSITY OF BRITISH COLUMBIA
(Vancouver)
December 2008

# ABSTRACT

Considerable research has been done to improve hydrate formation rate. One of the ideas is to introduce mechanical mixing which later tend to complicate the design and operation of the hydrate formation processes. Another approach is to add surfactant (promoter) that will improve the hydrate formation rate and also its storage capacity to be closer to the maximum hydrate storage capacity. Surfactant is widely known as a substance that can lower the surface or interfacial tension of the water when it is dissolved in it. Surfactants are known to increase gas hydrate formation rate, increase storage capacity of hydrates and also decrease induction time. However, the role that surfactant plays in hydrate crystal formation is not well understood. Therefore, understanding of the mechanism through morphology studies is one of the important aspects to be studied so that optimal industrial processes can be designed.

In the present study the effect of three commercially available anionic surfactants which differ in its alkyl chain length on the formation/dissociation of hydrate from a gas mixture of 90.5 % methane – 9.5% propane mixture was investigated. The surfactants used were sodium dodecyl sulfate (SDS), sodium tetradecyl sulfate (STS), and sodium hexadecyl sulfate (SHS). Memory water was used and the experiments for SDS were carried out at three different degrees of under-cooling and three different surfactant concentrations. In addition, the effect of the surfactant on storage capacity of gas into hydrate was assessed.

The morphology of the growing crystals and the gas consumption were observed during the experiments. The results show that branches of porous fibre-like crystals are formed instead of dendritic crystals in the absence of any additive. In addition, extensive hydrate crystal growth on the crystallizer walls is observed. Also a "mushy" hydrate instead of a thin crystal film appears at the gas/water interface. Finally, the addition of SDS with concentration range between 242ppm – 2200ppm ($\Delta T = 13.1^0C$) was found to increase the mole consumption for hydrate formation by 14.3 – 18.7 times. This increase is related to the change in hydrate morphology whereby a more porous hydrate forms with enhanced water/gas contacts.

# TABLE OF CONTENTS

# LIST OF TABLES

# LIST OF FIGURES

# ACKNOWLEDGEMENTS

First of all, I would like to thank God for His support and encouragement that He gave me during my Master program at UBC. I would also like to thank my supervisor, Dr. Peter Englezos for his patience in teaching me, for his ideas and guidance during the completion of this research project. I also want to thank for the support from my family (Putu Hindradata, Oei Mei Fie, Budi Yoslim, and Benny Yoslim).

I also want to express thanks to Cef Haligva, Praveen Linga, Rajnish Kumar, Robin Susilo, and Dr. Judong Lee for their brilliant ideas and great discussions.

Lastly, I would like to show gratitude for the financial support from *National Sciences and Engineering Research Council of Canada* (NSERC)

# Chapter 1: INTRODUCTION

Hydrates, which were first found by Sir Humpry Davy (1811), are non-stoichiometric ice-like structures which occur when water molecules attach themselves through hydrogen bonding and form cavities which can be occupied by a gas or volatile liquid molecule (Davidson, 1973; Ripmeester, 1987). It was not until nearly 100 years later that they were researched intensely due to pipeline blockage during oil and gas transport (Hammerschmidt, 1934). Gas hydrates have both problems and opportunities for the oil and gas industry. Traditionally, natural gas hydrates are considered as a nuisance in the oil and gas industry. However, on the other hand, there are a number of technologically important application areas of gas hydrates such as separation processes (Eick and Klara, 1990; Kang and Lee, 2000; Linga et al., 2008; Linga et al., 2007), fuel transportation and storage(Englezos and Lee, 2005; Gudmundsson, 1999; Gudmundsson, 1998; Gudmundsson, 2003; Mori, 2003; Okutani et al., 2008; Watanabe et al., 2005a; Zhong and Rogers, 2000). Moreover, gas hydrates were found to occur naturally in the sea bed and below permafrost which is believed to be a significant energy source for the future (Makogon and Tsarev, 1972; Sloan, 1990).

Gas hydrates are formed of two components; host and guest molecules. Water or ice molecules act as the host molecules and form the cages that will trap the guest molecules (gas) inside. Hydrates can trap gases like light hydrocarbons, carbon dioxide and light fluorocarbons where their molecular sizes are suitable for hydrate formation. Firstly in

hydrate formation, the host water molecules are used in forming the cage which entraps the gas. The hydrogen bonds between each water molecule help the cage to be formed. When the cage is formed, the gas has already been captured inside it. If there was no gas inside the cavity, then the cage would be unstable, however, the guest molecules inside increase the stability of the cage and prevent it from a potential collapse. The presence of guest gases can thermodynamically stabilize the ice-like structure via van der Waals forces without any chemical reaction. Gas hydrates form at a temperature higher than freezing point of water if an adequate high pressure of guest gas is applied. The equilibrium pressure and temperature for hydrate formation varies for different guest molecules.

In order to improve our understanding of gas hydrates, studies on the kinetics are very crucial and necessary. The studies of kinetics are achieved by different methods. These methods can be classified in two categories; macroscopic and microscopic measurements. Macroscopic measurements are larger-scaled measurements compared to microscopic measurements, which mostly focus on molecular-scale studies.

Macroscopic measurement and analysis of gas hydrates can be divided into two most common techniques which are gas uptake measurements (Englezos et al., 1987a; Englezos et al., 1987b; Linga et al., 2007) and morphology(Kumar et al., 2007; Lee et al., 2006; Ohmura et al., 2005; Ohmura et al., 2004; Okutani et al., 2008). Both gas uptake and morphology studies can provide information on the mechanistic aspect of crystal nucleation (induction time), rate of growth, and decomposition. Moreover, morphology studies involve observations of hydrate formation. As briefly mentioned before, microscopic measurements

focus on molecular-scale studies and provide information on the composition and the molecular structure of the sample. There are different types of microscopic measurements performed such as Raman spectroscopy, diffraction, and nuclear magnetic resonance (NMR) (Ripmeester and Ratcliffe, 1999; Sloan, 2003; Susilo et al., 2006; Susilo et al., 2007; Tulk et al., 2000).

## 1.1 Structure of Gas Hydrate

There are three well known structure of gas hydrates which are Structure I (sI), Structure II (sII) and Structure H (sH) (Davidson, 1973; Englezos, 1993a; Ripmeester et al., 1987; Sloan, 2003; Tulk et al., 2000). Each structure is a different combination of cages and water molecules. When two small pentagonal dodecahedral cages and six large tetrakaidecahedral cages are formed by 46 water molecules, structure I is formed. Structure II consists of 16 small pentagonal-dodecahedral cavities and 8 larger hexakaidecahedral cavities formed by 136 water molecules. Unlike these two structures, in Structure H, there are three sizes of cages and this structure consists of 3 small, 2 medium and 1 large sized cage formed by 34 water molecules. In addition, structure H hydrates require two different sizes of gas molecules in order to be stable whereas the other two types only need a single type of guest molecule in order to be stable. Due to that difference, Structure H hydrates are called double hydrates. Small guest molecules, such as xenon, methane or hydrogen sulfide, occupy the two small cages of the sH hydrate while a larger molecule occupies the large sH cage. This information and cage properties of the three hydrate structures are summarized in the following Figure 1.1.

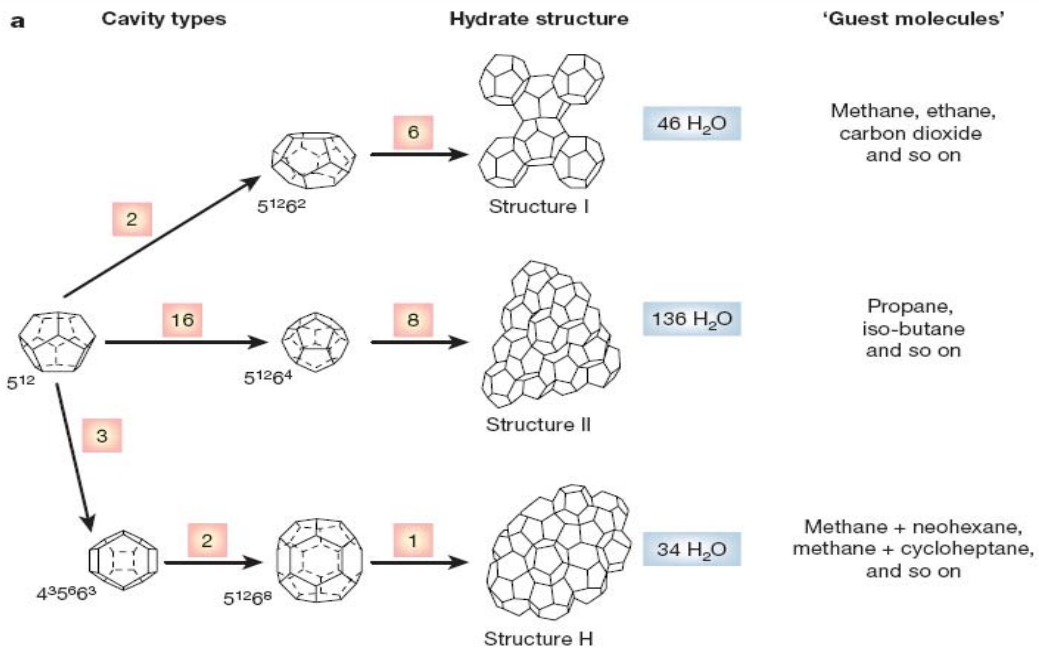


**b**

| Hydrate crystal structure | I | | II | | H | | |
|---|---|---|---|---|---|---|---|
| Cavity | Small | Large | Small | Large | Small | Medium | Large |
| Description | $5^{12}$ | $5^{12}6^2$ | $5^{12}$ | $5^{12}6^4$ | $5^{12}$ | $4^35^66^3$ | $5^{12}6^8$ |
| Number of cavities per unit cell | 2 | 6 | 16 | 8 | 3 | 2 | 1 |
| Average cavity radius (Å) | 3.95 | 4.33 | 3.91 | 4.73 | 3.91† | 4.06† | 5.71† |
| Coordination number* | 20 | 24 | 20 | 28 | 20 | 20 | 36 |
| Number of waters per unit cell | 46 | | 136 | | 34 | | |

*Number of oxygens at the periphery of each cavity.
†Estimates of structure H cavities from geometric models.

Figure 1.1: Geometry of hydrate cages for different structure (a), hydrates structure and properties (b)(Sloan, 2003)

As mentioned before, the structure of the hydrate depends on the size of the guest gas molecule and also the conditions of the surrounding area. For example, methane ($CH_4$) has the ability to form both structure I and structure II, however, extreme pressure values are necessary in order to form structure II. Therefore, most of the time methane forms structure I in nature. Some other basic gases that form structure I based on their molecule sizes are ethane ($C_2H_6$), carbon monoxide (CO), and carbon dioxide ($CO_2$).

The structure II transition occurs when two molecules are at each extreme of the structure I molecular sizes (Koh, 2002). That is, small structure I formers in the $5^{12}$ cage (which are almost small enough to form structure II) and large structure I formers in the $5^{12}6^2$ cage (which are almost large enough to form structure II) will, when mixed, cause structure II to form from two structure I formers (Sloan, 2003). Propane ($C_3H_8$), oxygen ($O_2$), nitrogen ($N_2$), and hydrogen (H2), can be given as the examples of structure II hydrates.

The formation of structure H requires the cooperation of two guest gases (large and small) to be stable. It is the large cavity that allows structure H hydrates to fit in large molecules, given the presence of other smaller help gases to fill and support the remaining cavities.

Natural Gas mostly consists of light hydrocarbon molecules, such as methane ($CH_4$), ethane ($C_2H_6$), and propane ($C_3H_8$). Of the two crystalline structures for gas hydrates, $CH_4$ hydrate and $C_2H_6$ hydrate form structure I hydrates (sI), and larger guest molecules such as $C_3H_8$ form structure II hydrates (sII). In addition, gas hydrates are only stable under high-pressure and low-temperature conditions.

For mixtures of such gases, both the equilibrium conditions and the structures of the resulting gas hydrates are rather complicated, sensitive functions of the conditions of the gas compositions. For example, gas hydrates formed from gas mixtures of $CH_4$ with small amounts of $C_3H_8$ are expected to form sII at lower pressures than the pure $CH_4$ hydrate (van der Waals and Platteeuw, 1959). In this hydrate, $C_3H_8$ molecules occupy only the large cage, whereas $CH_4$ molecules exist in the remaining cages (both small and large cages) of

the sII hydrate, a structure that was predicted from solid solution theory (van der Waals and Platteeuw, 1959) and confirmed by NMR measurements(Ripmeester and Ratcliffe, 1988a). Mixtures of $CH_4$ and $C_2H_6$ are also found to form both sI and sII hydrate, depending on the vapor composition in equilibrium with the hydrate phase.

When such gas mixtures combine with water in a batch-type reactor to form hydrate, guest composition changes during hydrate formation and the crystal structure may also change. Even though hydrate samples have been prepared using such a batch-type reactor in many studies, this complicated process is not understood well enough to accurately know the physical properties of the sample. A better understanding of the formation of mixed gas hydrates in a batch-type reactor may also help us to determine the feasibility of using gas hydrates for natural gas storage and transportation.

For this purposes, Uchida et al. (2004) and Kumar et al.(2008) have done an experiment with a crystallizer connected to a gas chromatograph (GC) to measure the composition change in the vapour phase containing natural gas simulating light hydrocarbon ($CH_4$ , $C_2H_6$ and $C_3H_8$). In agreement with thermodynamics, the final vapor compositions were further enriched in $CH_4$ over those in the initial compositions. However, GC measurements and the drop in pressure indicated that the mixed-gas hydrate formation had two steps. The two-step formation process was recognized by a temporary period of nearly constant pressure after the vapor composition became rich in $CH_4$. Both X-ray diffraction (XRD) and Raman spectroscopic analyses were done on several $CH_4$-$C_3H_8$ hydrate samples by Uchida et al. (2004) to characterize the hydrates in each step of the two-step formation process. $CH_4$ and

$C_3H_8$ mixed gas hydrate with structure II formed at the first step, whereas almost pure $CH_4$ hydrates with structure I formed in the second step. These results were also confirmed by Kumar et al. (2008) using three solid-state analytical tools (PXRD, NMR and Raman).

## 1.2 Importance of Gas Hydrate Studies

Initially, hydrates which are also known as clathrate hydrates were recognized as a source of problem in oil and gas production(Hammerschmidt, 1934; Katz, 1959; Katz, 1991). In addition to problems, there are a number of technologically important applications of gas hydrates such as in separation processes (Knox et al., 1961; Ngan and Englezos, 1996), $CO_2$ Capture and Sequestration (Linga et al., 2008; Linga et al., 2007), fuel transportation and storage (Gudmundsson, 1999; Gudmundsson, 1998; Gudmundsson, 2003; Gudmundsson et al., 2002; Klein Nagelvoort, 2000; Taylor, 2001). Moreover; gas hydrate is found in sub-oceanic sediments in the Polar Regions and in continental slope sediments, as a future source for energy (Makogon and Tsarev, 1972; Sloan, 1990) and also as a source of green house gases (Englezos, 1993b).

### 1.2.1 Hydrate Plug Prevention

The formation of clathrate hydrates in the natural gas/ oil pipelines has long been a serious problem in gas/oil industries and a best prevention solution still needs to be found. Hydrates can form plugs in pipelines under low temperature, and high pressure conditions and cause a significant production loss. This past decade, the oil and gas industry started to move into deep water exploration and production, where pressure and temperature condition are better

for hydrate formation. This phenomenon has brought scientists, engineers and many others to find a way to prevent hydrate formation during transportation.

As discussed before, natural gas hydrates can form under certain temperature and pressure conditions. To satisfy these conditions (low temperature and high pressure) is easy in nature and in the oil and gas industry. Natural gas pipelines, especially the ones going underneath the ocean provide perfect conditions for such processes since the temperature and temperature are suitable for hydrates formation. Therefore, this is a huge issue for the oil/gas industry since hydrate formation occurring clogs the pipelines and cause potential safety threats and danger for gas to leak into the atmosphere. Considering the significant economic risks in the gas and oil industry (Hansen, 1999), a great deal of research has been conducted by the petroleum industry in order to prevent this phenomenon. As mentioned before that hydrates can form when there is enough pressure, appropriate temperature and water is available, so one of the traditional way to prevent hydrate formation is to process the petroleum fluids, usually by increasing the fluid temperature, decreasing the working pressure, and/or removing water content. Another traditional and well-established and the most common method to avoid hydrate from forming is to inject thermodynamic inhibitors such as methanol, glycol that will shift the equilibrium conditions of hydrate formation so that higher pressure and lower temperature can be accommodated (Dholabhai, 1992; Sloan, 1998).

Currently, the search for new inhibitors (kinetic inhibitor and anti-agglomerates) is motivated by the high cost of thermodynamic inhibitors in offshore applications where

extreme pressure and temperature conditions occur (Fu, 2002; Huo et al., 2001; Lovell, 2003; Mehta, 2002). Kinetic inhibitors do not work by shifting the equilibrium conditions of hydrate formation such as thermodynamic inhibitors, instead they work by delaying the formation of hydrates or by decreasing the rate at which hydrate forms, preventing plugs for a period of times. Moreover, anti-agglomerants work by allowing hydrates to form but not to agglomerate so that hydrate deposition and plugging can be prevented.

Several types of kinetic inhibitors that have been recognized as an effective inhibitors are poly (N-vinylcaprolactam) known as PVCap, and poly (N-vinylpyrrolidone) known as PVP. The trend nowadays in using kinetic inhibitors is to abandon the use of synthetic chemicals like PVP and to switch to environmental friendly inhibitors that have been engineered by evolutionary processes in organism over the millennia. Professor Walker's group at Queens University and in collaboration with the National Research Council of Canada has recently discovered that fish and insect antifreeze proteins (AFPs) not only bind to ice but also inhibit gas hydrate crystallization (Zeng et al., 2006a; Zeng, 2005; Zeng et al., 2006b). This is a significant finding since it represents an environmentally-benign method to control and inhibit hydrate formation.

### 1.2.2 Carbon Dioxide Capture and Sequestration

GHG (greenhouse gases) such as carbon dioxide, and methane have been a major issue nowadays that cause temperature increase in this world (global warming). Most of the GHG is coming from usage of fossil fuels and it is estimated that the usage will keep increasing in these coming years (WEO, 2007).

Global warming is not a trivial issue because it is likely to cause severe consequences to the physical and chemical processes and biological life on earth. In order to prevent global warming while keeping social and economic growth, actions to reduce or eliminate GHG's emission are needed and numerous technologies are being considered for $CO_2$ capture such as cryogenic distillation, absorption, use of solid adsorbents and gas hydrate (Aaron and Tsouris, 2005; Kang and Lee, 2000; Metz, 2005; Voormeij and Simandl, 2004). As one of the technologies available for CO2 capture, gas hydrate is still a subject of active research to improve the efficiency and to reduce the operating cost (Kang and Lee, 2000; Linga et al., 2008) for GHG capture.

### 1.2.3 Future Energy Source

Methane hydrates has been identified as energy source for the next generation and it is believed that the amount of carbon sequestered both offshore and onshore to be larger than the sum of the energy of all other fossil fuels on earth (Kvenvolden, 1988). In addition, it is also noted that methane hydrates are distributed evenly worldwide (see Figure 1.2) (Makogon et al., 2007).

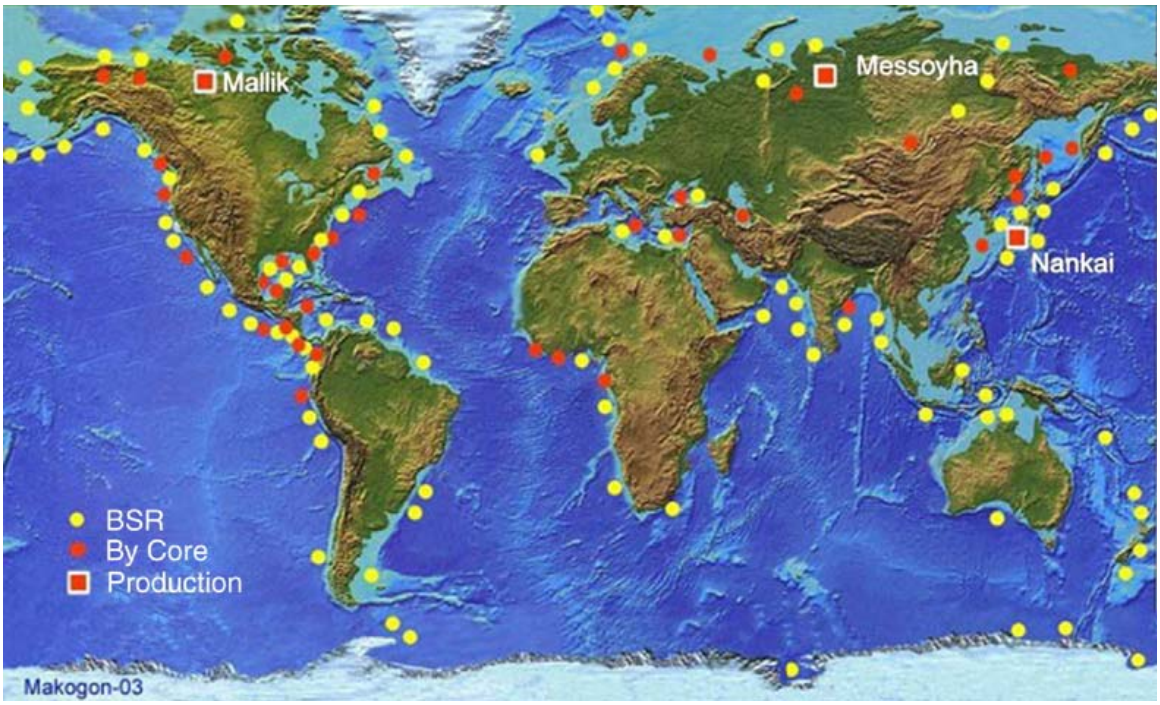


Figure 1.2: Map of discovered gas-hydrate deposits, reprinted from (Makogon et al., 2007), with permission from Elsevier.

Currently, there are three main techniques to recover methane from hydrates which are: depressurization, thermal stimulation and injection of inhibitors. Depressurization and thermal stimulation work by lowering the pressure and by increasing the temperature of the fluids respectively, so that the conditions are out from the hydrate stability region. Moreover, injection of inhibitor works by shifting the methane hydrate phase diagram so that hydrates will be stable only at a higher pressure and/or lower temperature.

In both 1998 and 2002, two test wells in the Mackenzie Delta, Canada were drilled and provided useful information on how to produce gas from hydrate. This knowledge will eventually help to develop more efficient and less expensive methods to extract gas from hydrates.

### 1.2.4 Gas Hydrate Technology and Natural Gas Storage & Transport

Storing and transporting natural gas as hydrates from stranded gas fields is one of the most promising applications of gas hydrates. Current investigations show that there are 40-60% of natural gas fields worldwide that are considered as stranded or abandoned gas fields (Ivanhoe, 1993). Stranded and abandoned gas fields refer to gas fields where no pipeline capacity is available, no gas user is available and the building of new infrastructure will be too expensive. Thus, it is not economically profitable to extract the gas with current technologies due to location (remote area), quantities (volume), and production cost.

Most well known methods to transport natural gas are through pipelines or in liquefied form (LNG). Both of these methods are known to have high fixed and capital cost. In order to be profitable to extract gas from stranded and abandoned gas fields, new technologies to store and transport are needed.

There are a few "new" alternatives under investigation in order to store and transport natural gas. Natural Gas Hydrates (NGH) is one of the "new" methods. However there are not well-established and thus further investigations is still needed. One of the challenges is to find the most stable, effective and efficient way to transform gas into hydrate so that hydrate will form at the fastest rate and with the highest water to hydrate conversion while keeping the hydrate stable under the cheapest conditions (higher temperature and lower pressure). Compared to Liquefied Natural Gas (LNG), NGH is found to be easier to handle, safer and eco-friendly. NGH is easier to handle because hydrates can be stabilized at -20$^{o}$C and atmospheric pressure compared to LNG stabilized at -160$^{o}$C and atmospheric pressure. It is

safer because in hydrates, gas molecules are trapped inside cages formed from water molecules so that it minimizes chances of explosion. In addition, NGH is also more eco-friendly compared to LNG because it consumes less energy during production, and no hazardous substance is discharge during re-gasification. Although the gas storage density in liquefied natural gas (~600 v/v) is actually higher compared to natural gas hydrate (~170 v/v), NGH can be more economical at shorter distances and capacity compared to LNG in storing and transporting natural gas from a stranded or abandoned gas fields due to its lower initial capital cost and fixed cost (Gudmundsson et al., 2002).

Mitsui Engineering and Shipbuilding Corp., Inc (MES) has made a big step forward in order to commercialize natural gas hydrate technology by building a hydrate production pilot plant which is able to produce 600 kg of hydrate per day. MES also has an illustration on how to store and transport natural gas which is shown in Figure 1.3.

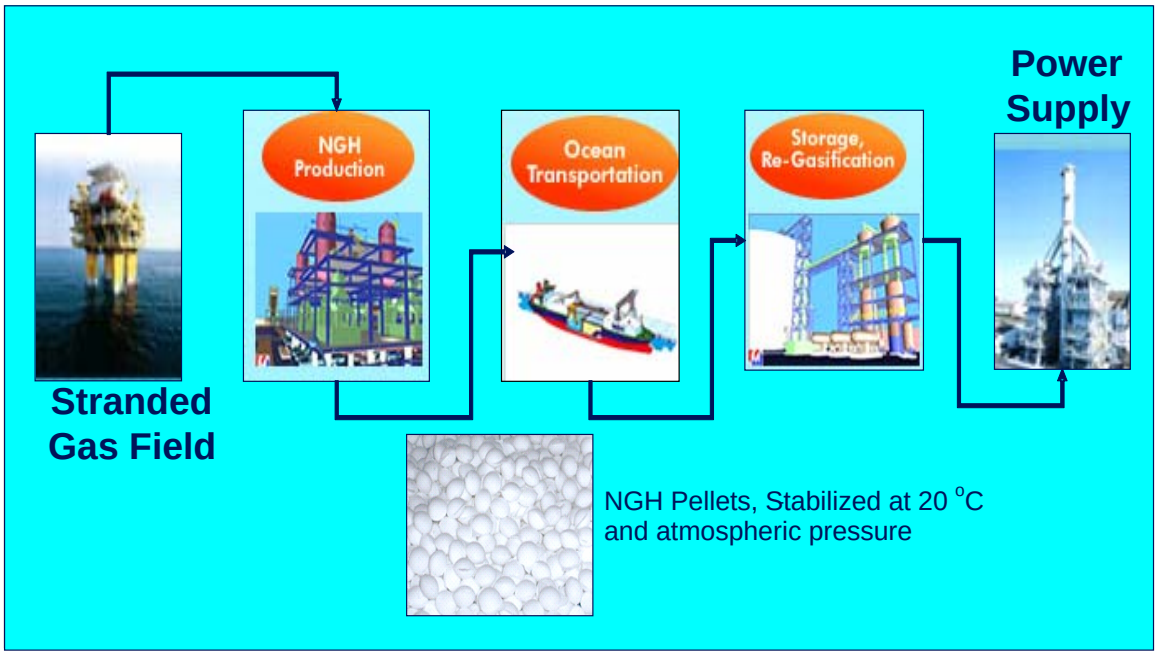


Figure 1.3: Natural Gas storage and transport illustrations from the gas field to the energy consumers in the form of hydrate pellets, © by Mitsui Engineering & Shipbuilding Co.,Ltd.

# Chapter 2: LITERATURE REVIEW & RESEARCH OBJECTIVES

Gas hydrates have unique gas storage properties, as one standard volume of hydrate can contain around 180 standard volumes of natural gas. This unique property of gas hydrates becomes appealing for industry to implement natural gas hydrate technology for storage and transportation. However, industrial applications of gas hydrate for storage and transport have been hindered by problems that effect the economics of process scale-up.

The problems are:

- Slow formation rates
- Unreacted interstitial water between hydrate crystals which become the highest mass/weight contribution
- Proper design of hydrate packing and ways to separate hydrates from unreacted water

Further investigations have been done to improve the formation rates and also decrease the unreacted interstitial water by adding a promoter such as surfactant. Comparison on the formation rates and morphology of system with and without additives are shown below and followed by research objectives.

## 2.1 System without Additives

As mentioned before that slow formation rates is one of the major problem that has to be overcome in order to implement gas hydrate technology for natural gas storage and transport.

### 2.1.1 Formation Rates in System without Additives

The mechanism of hydrate formation in a quiescent water-gas system (with no additives) appears to be that hydrogen-bonded configured water molecules cluster with solutes of hydrocarbon gas, proceeding to gather gas in the clusters until concentrations and sizes of the clusters are reached to give critical nuclei for hydrate crystal formation (Vysniauskas and Bishnoi, 1983). The induction time of hydrate formation depend on the system conditions, or in other words the induction time will be shorter when higher pressure or lower temperature is applied to the system. After an induction time, crystal growth is initiated by the formation of a hydrate film at the interface between liquid water and the adjacent gas (Lee et al., 2006). Once the interface is covered with crystals, the hydrate formation rate in the quiescent system is slow, for gas and water must diffuse through the film to maintain crystal growth. Formation rates becomes controlled by the diffusion rate through the hydrate film (Mori, 1996), which effectively isolates the gas from the water (Herri et al., 1996).

In order not to form hydrate crystals at the interface of gas and liquid so that continuous hydrate formation can be maintained, agitation of the water can be introduced. In the experimental apparatus of Narita and Uchida (1996) an impeller speed of 500 rpm gave a maximum hydrate reaction rate. Although high formation rates can be achieved with stirred

systems, this is not practical to be used in industrial sized process. Energy costs from stirring increases as the slurry thickens. In fact, thickening slurry in stirred system may limit the hydrate mass in the water to as low as 5 weight % (Vysniauskas and Bishnoi, 1983), at which an extra cost for the time of filtering and clarification would be necessary. The separation of hydrates from slurry requires additional labour as does the packing the hydrates in as storage vessel.

During hydrate formation, whether in a quiescent or stirred system, free water has been found to be trapped between solid hydrate particles. The water may represent a large percentage of the hydrate volume. Englezos (1996) found only 1.4-14% of the water after hydrate formation in an experimental cell (based on maximum amount that could form hydrates and dependent on the guest molecular identity) was bound in the hydrate structure while most of the water was trapped between solid particles. The entrapment is especially important for scaling up to a hydrate gas- storage process. For example, if gas storage in hydrates for industrial use were the goal, appreciable volumes of the storage tank would be occupied by the trapped unreacted water having no occluded gas.

### 2.1.2 Morphology of Clathrate Hydrate Crystal Growth in System without Additives

The morphology of gas hydrates ,which is the study of hydrate crystal growth at dimensions larger than the molecular size but much smaller than the dimensions of the system, is used to help understand the mechanistic aspects of gas hydrate formation and the results can be used to design a better process.

According to Ohmura et al. (2004) natural gas hydrates and $CO_2$ hydrates start to form at the interface of gas/water. The induction time and the morphology were found to be dependent on the driving force. The driving force can be explained as the temperature difference or the degree of under-cooling ($\Delta T = T_{eq}-T_{exp}$) between the experimental temperature and the equilibrium temperature or the pressure difference between the experimental pressure with the equilibrium pressure ($\Delta P = P_{eq}-P_{exp}$). The equilibrium pressure can be calculated by classic hydrate phase equilibrium calculation using software such as CSMHYD (Sloan, 1998).

Ohmura et al. (2005) reported a visual study of the formation and growth of clathrate hydrate crystals in liquid water without any additives and in contact with 99.9% methane gas under different pressure (6-10MPa) at a temperature of 273.5 K. Distinct variations in the morphology of hydrate crystals grown in liquid water were observed to be dependent on the driving force (pressure difference in this case). At pressures of 6-8 MPa, hydrate crystals with skeletal, columnar morphology (Figure 2.1) were observed. At pressure of 10 MPa, dendritic crystals were observed instead of skeletal, columnar crystals (Figure 2.2).

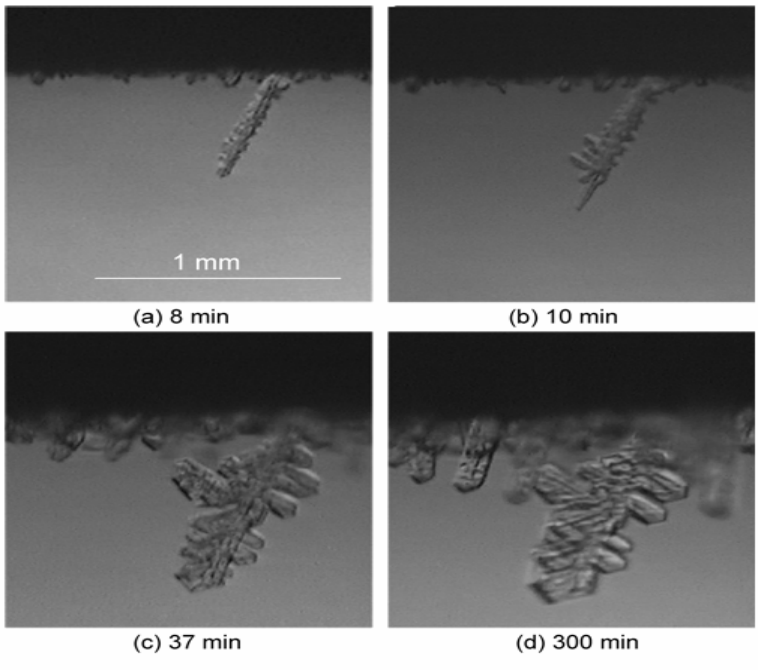


Figure 2.1: Sequential videographs of the growth of methane-hydrate crystals into liquid water presaturated with methane. p = 8.2 MPa, T = 273.7 K. The time lapse after the hydrate nucleation at the methane-water interface is indicated below each videograph (Ohmura et al. 2005).

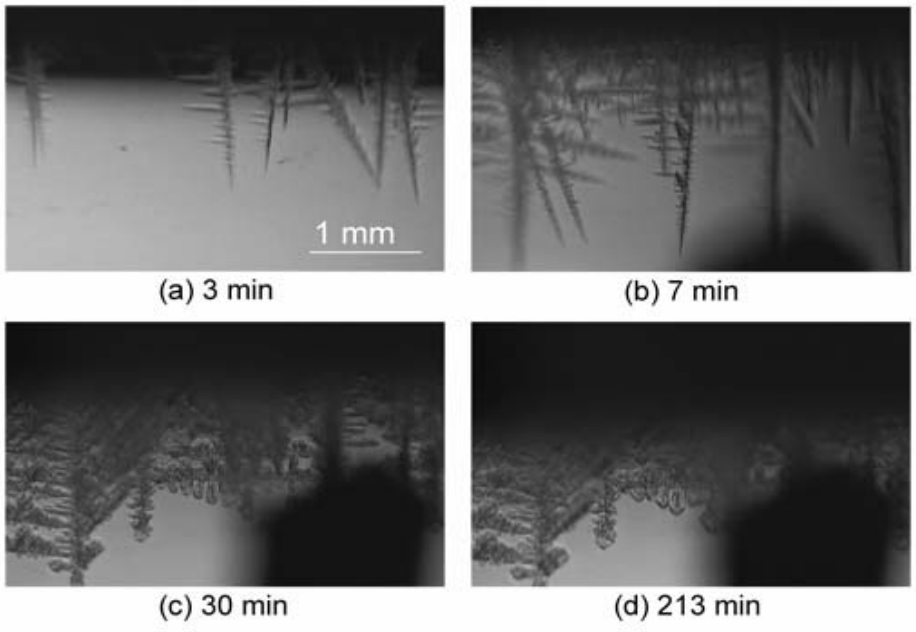


Figure 2.2: Sequential videographs of the growth of dendritic methane-hydrate crystals into liquid water presaturated with methane. p = 9.7 MPa, T = 273.3 K. The time lapse after the hydrate nucleation at the methane-water interface is indicated below each videograph (Ohmura et al. 2005).

Lee et al.(2006) observed system with a different gas mixture and a different driving force ($\Delta T$ = 15.2, 13.7, 8.1 and 3.2). The gas mixtures used were methane/propane with 90.5% methane and 9.5% propane which is known to form structure II hydrate. This mixture of hydrocarbon is a natural gas simulating light hydrocarbons. In most of the experimental runs, hydrate crystal growth similar to that previously reported in the systems with $CO_2$, fluorocarbons, and methane were found. Hydrate crystals first formed as a hydrate film at top surface of liquid water and gas. When under-cooling ($\Delta T < 3.2$), there is no significant hydrate growth that can be seen from the hydrate film, but columnar hydrate crystal can be found to grow below the hydrate film (Figure 2.3).

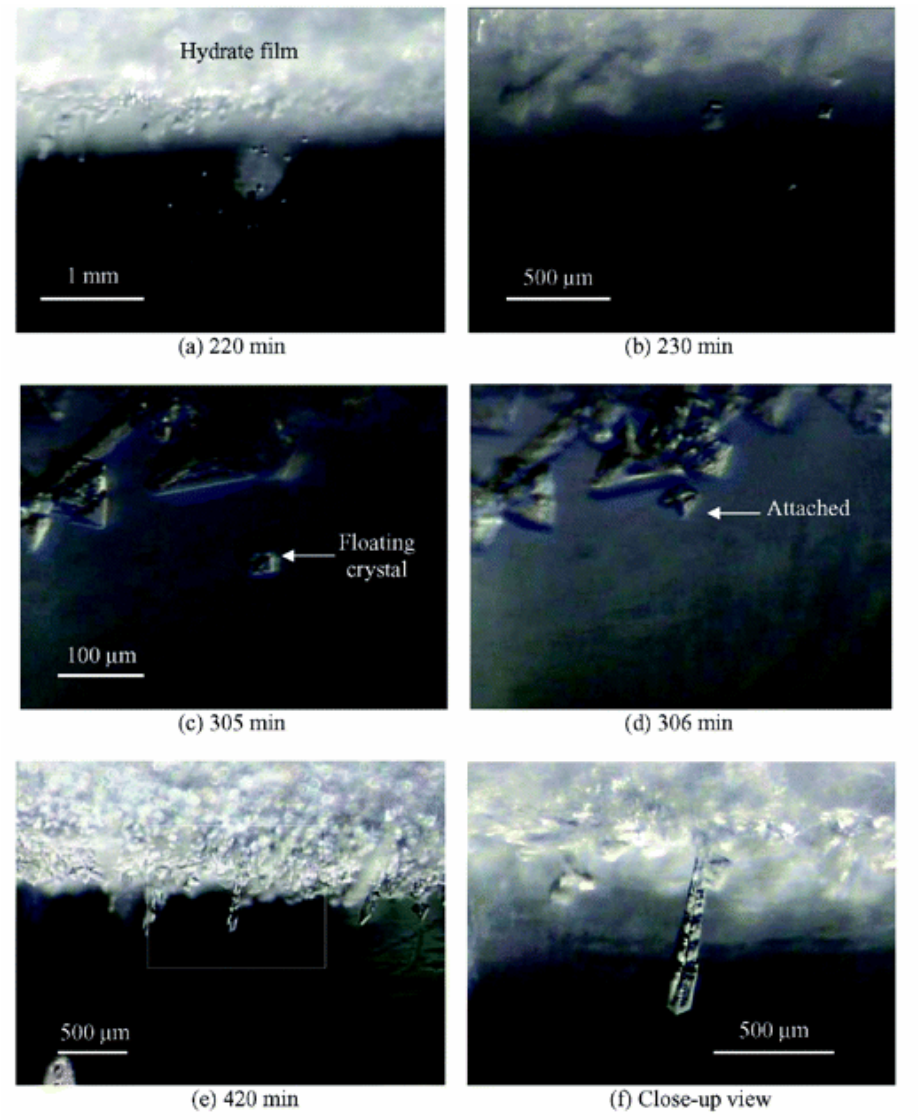


Figure 2.3: Sequential images of the crystals during hydrate formation from the methane-propane-water system at 1.43 MPa, 278.7K and 3.2 K under-cooling. The time lapse after the formation of hydrate film is indicated below each image. Image (f) is magnified from (e). (Lee et al. 2006)

The morphology of methane/propane hydrate crystal during formation at intermediate degrees of undercooling is different from the lowest degree of under-cooling. Needle-like hydrate which later turns to dendritic shapes grows downward into the bulk water from the hydrate film (Figure 2.4). As degrees of under-cooling increase, the downward crystal grows with a higher rate and with finer spacing.

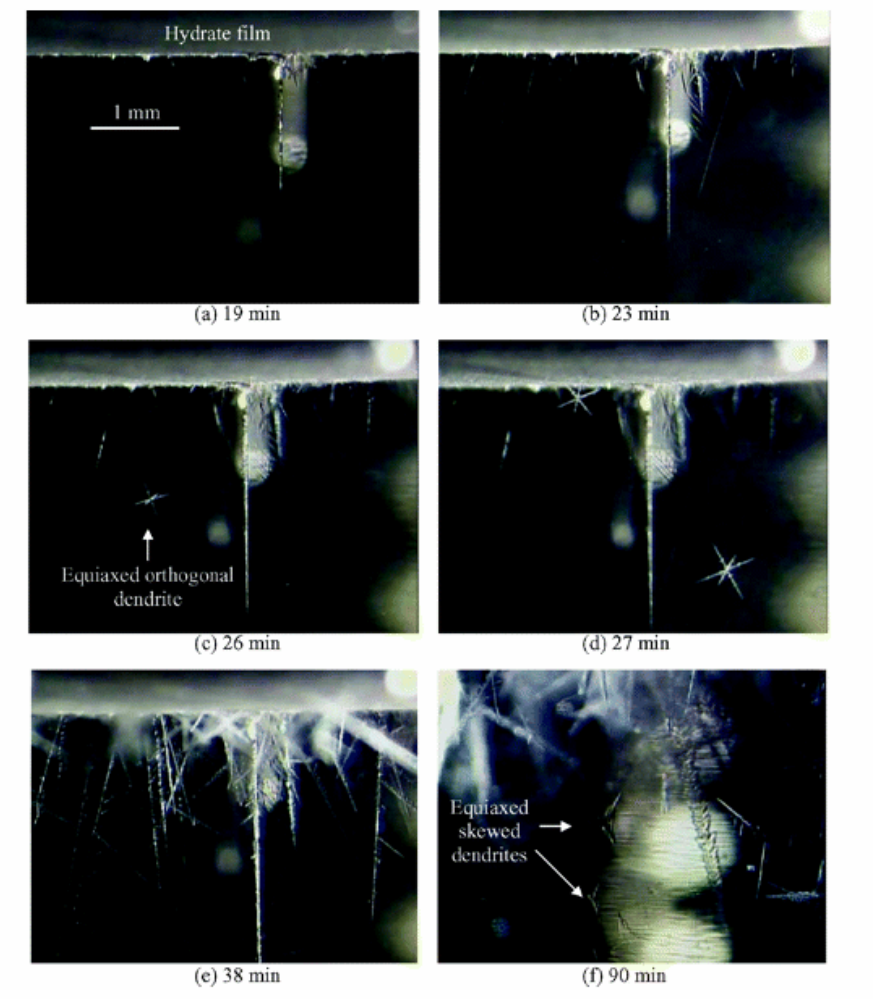


Figure 2.4: Sequential images of the crystals during hydrate formation from the methane-propane-water system at 3.22 MPa, T = 274.9 and 13.7 K under-cooling. The time lapse after the formation of hydrate film is indicated below each image.

## *2.2 System with Additives*

There are two main reasons for using additives for hydrate formation processes in which their goals are totally opposite:

- Additives to prevent hydrate plugs during oil and gas production (Flow Assurance)
- Additives to speed up the formation rate of hydrate for storage and transportation purposes

Massive efforts have been made to find new additives that are economical, environmentally friendly and that can inhibit hydrate growth or the prevention of agglomeration during oil and gas production. Some morphological studies on the effect of polymeric inhibitor have also been made by Kumar et al (2007). One of the latest and most promising findings of additives that can prevent hydrate formation is the use of Antifreeze proteins from certain vertebrates, fungi, plants and bacteria. Antifreeze proteins (AFP) are a class of polypeptides that functioned to allow certain vertebrates, fungi, plants and bacteria to survive in subzero environments. AFP is known to kinetically inhibit hydrate formation and eliminate the existence of a memory effect that sometimes causes more problems for the oil and gas industry (Zeng et al., 2006a; Zeng et al., 2007; Zeng et al., 2003; Zeng et al., 2006b).

This work is concerned with additives that speed up the formation rate such as surfactants. As surfactant is a substance that can lower the surface or interfacial tension of the medium in which it is dissolved. The surfactant that promoted hydrate growth was first found by Kalogerakis et al. (1993) during screening of surface active agents for preventing hydrate formation in the oil and gas production. So far, surfactants are known to effect the formation rate, storage capacity, induction time, and mechanism of hydrate formation.

### 2.2.1 Effect of Surfactant on Formation Rates and Gas Storage Capacity of Hydrates

In the early study of surfactants, Kalogerakis et al. (1993) observed the effect of surfactants on the kinetics of methane hydrate formation. They reported that surfactant does not influence the thermodynamics; however, they have a strong influence on increasing the overall rate of hydrate formation. Another observation made is that the hydrate particles that formed in a system with various surfactants exhibits diverse agglomeration characteristics. Zhong and Rogers(2000) also reported that addition of a surfactant can increase the formation rate of ethane hydrate in a quiescent system (Figure 2.5).

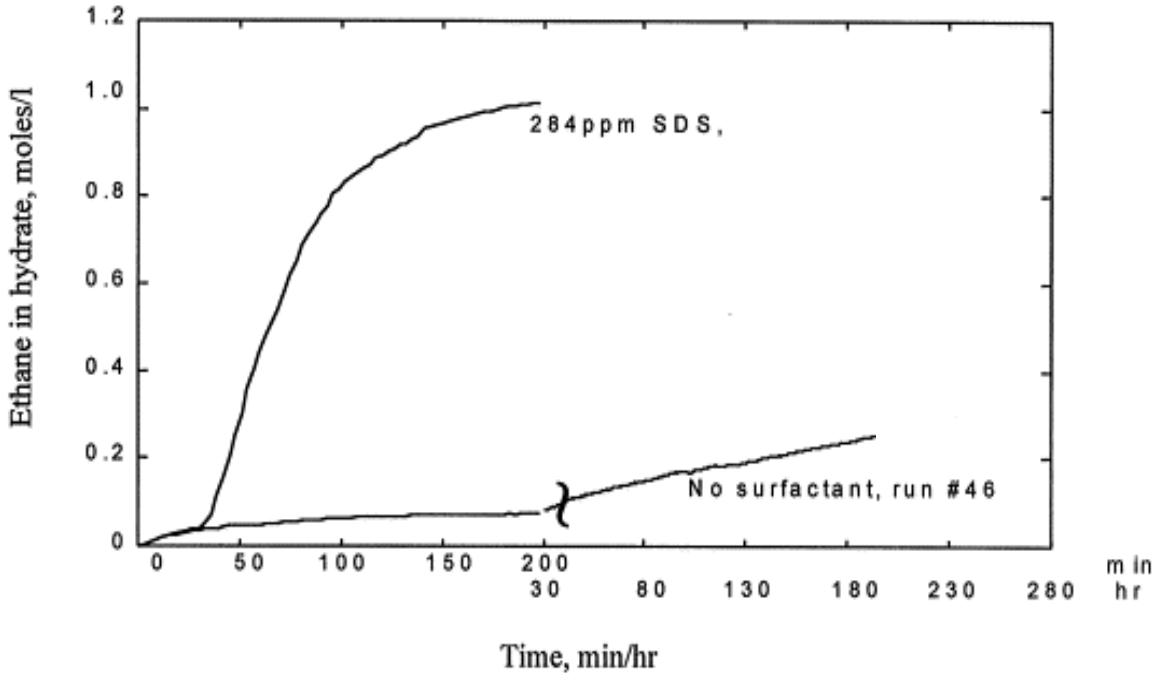


Figure 2.5: Surfactant increases formation rate of ethane hydrate in quiescent system(Zhong and Rogers, 2000).

There are three major types of surfactant which are non-ionic, anionic and cationic surfactant. Non-ionic surfactants are surfactants which do not dissociate in water, and an anionic/cationic surfactant dissociates in water and has an anionic/cationic hydrophilic group. Karaaslan and Parlaktuna (2000) and Sun et al. (Sun et al., 2003a; 2003b) observed the effect of different types of surfactant on the hydrate formation rate and assessed the hydrate storage capacity. Both papers reported that the anionic surfactants are more promising compared to cationic, non-ionic and a mixture of anionic with non-ionic surfactants (Figure 2.6).

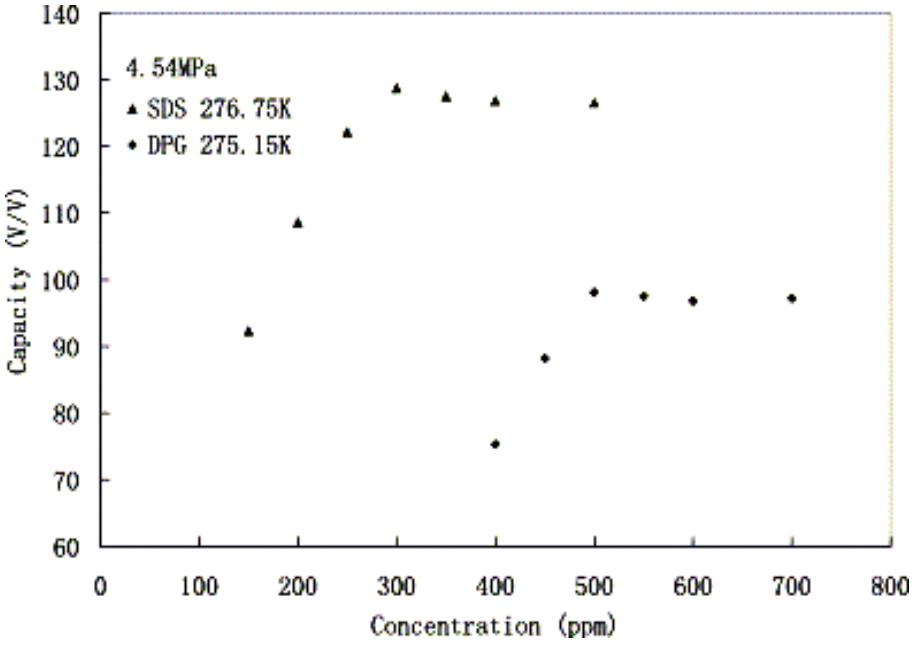


Figure 2.6: Gas storage capacity in hydrates comparing anionic with non-ionic surfactant at different concentration (Sun et al., 2003a)

Karaaslan et al. (2002) observed the effect of anionic surfactants on different types of hydrate structures. In this paper, he concluded that anionic surfactants increase the hydrate formation rate of both sI and sII hydrate structures, but its effect on sI is more significant than on sII.

Link et al.(2003) compared several anionic and cationic surfactants for their ability to enhance the uptake of methane for hydrate formation. In order to decide which surfactant actually works the best, there is one parameter that can be compared which is percent uptake. 100 percent uptake means that all the water available turns into hydrate. The higher the percent uptake, the better the surfactant is. In this paper, it was found that Sodium Dodecyl Sulfate (SDS) gives the best performance (Table 2.1).

Table 2.1: Comparison of percent uptake measurement of different surfactants (Link et al., 2003)

| Surfactant | Percent uptake |
|---|---|
| Dodecyl trimethyl ammonium chloride | 13.9 |
| Sodium dodecyl sulfate | 97.3 |
| Dodecylamine | 9.9 |
| Dodecylamine HCl | 11.9 |
| Sodium lauric acid | 77.4 |
| Sodium oleate | 70.5 |
| Superfloc 16® | 19.6 |
| Superfloc 84® | 20.1 |

#### 2.2.1.1 Effect of surfactant concentration and carbon chain length on hydrate formation kinetics and storage capacity

The effect of SDS surfactant concentration ranged from zero to 2000 ppm on the formation rates and the storage capacity of methane hydrate was observed by Lin et al. (2004). It was observed that the higher SDS concentration, the earlier hydrate formation rates slowed down due to most of the water having been converted to hydrate (Figure 2.7). Hydrate storage capacity is maximized at 650 ppm of Sodium Dodecyl Sulfate (Figure 2.8).

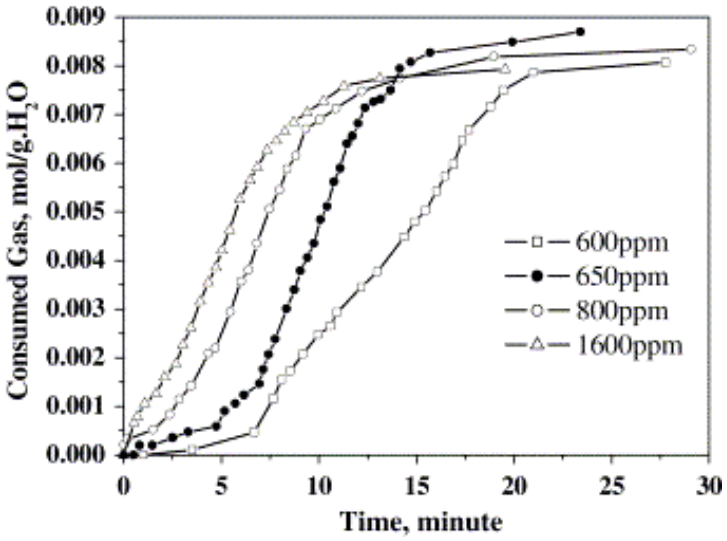


Figure 2.7: The accumulative moles of gas consumed per gram of water as a function of time during the growth period of hydrate formation with respect to different SDS concentrations in initial aqueous solution at 276K and 6.6 MPa (Lin et al., 2004).

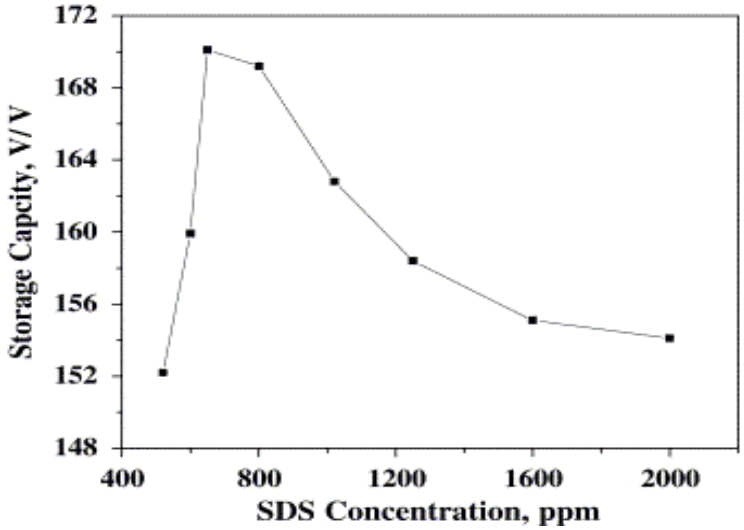


Figure 2.8: Influence of SDS concentrations on hydrate storage capacity at 276K and 6.6 MPa (Lin et al., 2004).

Daimaru et al. (2007) tested three surfactants with sodium sulfonic acid groups but with differences in their carbon chain length (C4, C12, and C18). They observed that the formation rate of xenon hydrate was accelerated at a lower range of surfactant concentration up to a point where the increase in concentration reduced the formation rate for all three surfactants tested. Another observation made in this report is that all three surfactants increased the formation rate but the C4 surfactant gives the most significant increase compared to the other two. Okutani et al. (2008) also investigated three different types of sodium alkyl sulfates (C12, C14, and C16) and their experimental results show that C12 and C14 can increase the formation rate and gas storage capacity equally but the concentration needed for C14 is less than that for C12.

### 2.2.2 Effect of Surfactant on Induction Time and Mechanism of Hydrate Formation

According to Zhong and Rogers (2000), addition of surfactant also decreases the induction time. At 242 ppm SDS, a significant change in hydrate induction time occurs which defines the CMC. If the surfactant solution exceeds this concentration of 242 ppm, hydrates develop extremely fast in a quiescent system (Figure 2.9).

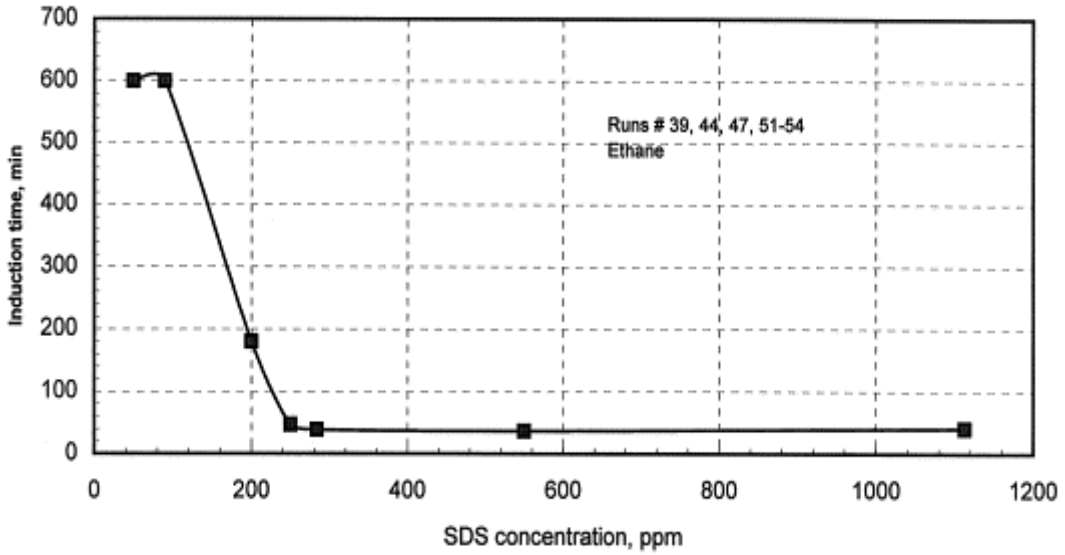


Figure 2.9: Effect of surfactant concentration on the induction time of ethane hydrates (Zhong and Rogers 2000).

The first mechanism of hydrate growth when surfactant is present in the system was proposed by Kutergin et al. (1992) and Mel'nikov et al. (1998). They reported that addition of surfactant to the liquid water caused morphological changes in the hydrate film so that the gas-water contact can be continuously maintained until most of the water converted to hydrate. Gas-water contact can be maintained because hydrate crystals no longer formed a dense, rift-less film at the interface of gas-liquid but migrated to the vertical chamber walls and formed relatively thick, porous hydrate layers which grew upward. This continuous grow along the crystallizer wall indicates that the SDS solution was sucked into the porous

hydrate layer to flow upward through the pores inside the layer by the action of a capillary force.

Besides this "capillarity-driven hydrate formation mechanism", R E Rogers and his coworkers (Rogers et al., 2005; Zhong and Rogers, 2000) proposed a surfactant micelle hypothesis. This hypothesis stated that surfactant micelles formed in the aqueous phase and that this strongly affected the increase in hydrate formation rate. However, this hypothesis was disputed in some recent papers(Di Profio et al., 2005; Di Profio et al., 2007; Gayet et al., 2005; Watanabe et al., 2005a; Watanabe et al., 2005b; Zhang et al., 2007). Based on these papers, it is confident to state that SDS does not form micelles under thermodynamic conditions generally set in hydrate forming operations irrespective of its concentration.

Recently, Okutani et al. (2008) reported qualitative observations of hydrate growth and concluded that it is in qualitative agreement with the description given by Kutergin et al.(1992), Mel'nikov et al.(1998), Zhong and Rogers (2000), Watanabe et al. (2005b), and Gayet et al. (2005). The above work suggested that the capillary-driven water suction that allows water to flow upward through the porous hydrate layer is responsible for enhanced hydrate formation when surfactant is present in the system. Another observation made by Okutani et al. (2008) is that there is no distinct qualitative difference in hydrate growth behaviour with various surfactant types with different alkyl chain length and the surfactant concentration used (~100ppm - ~ 4000ppm).

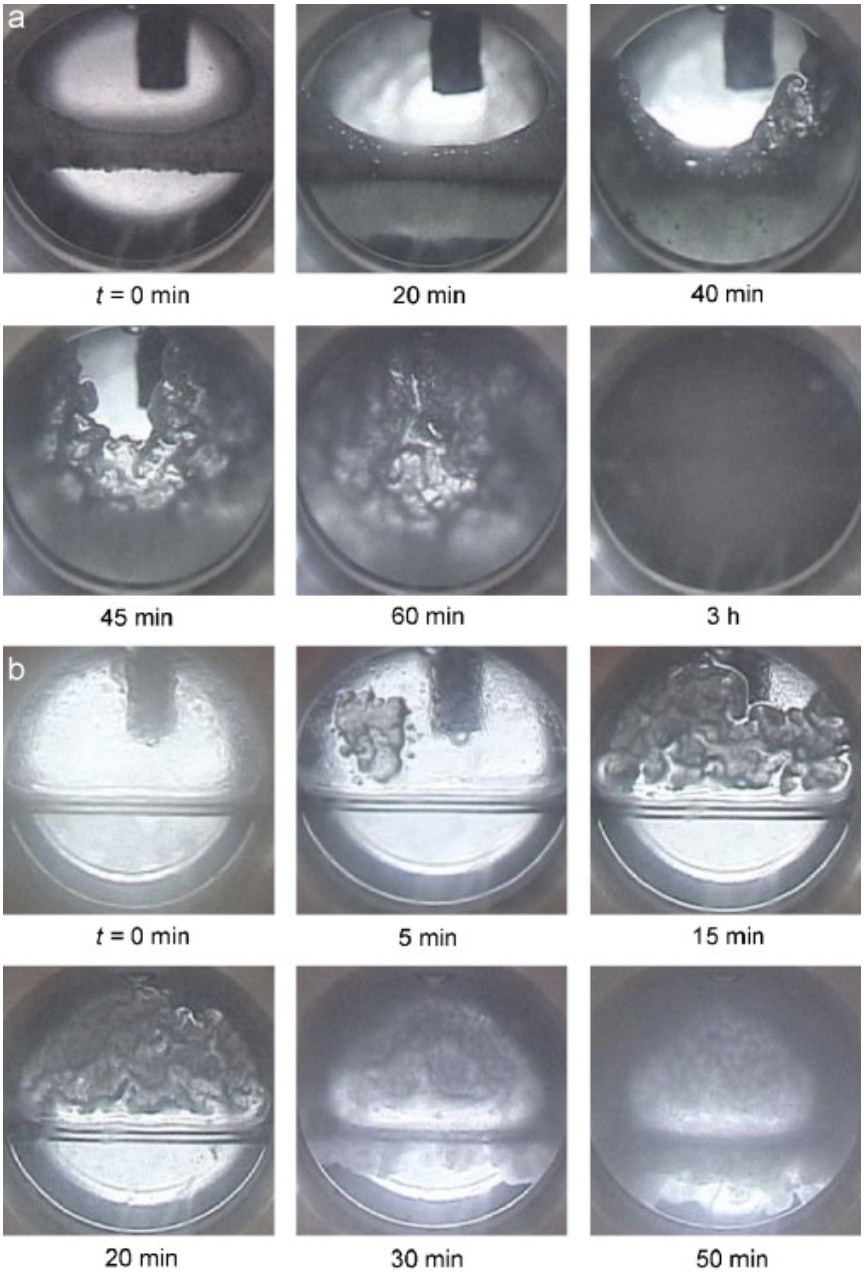


Figure 2.10: The typical sequences of hydrate-phase growth observed with a horizontal camera axis through a 30-mm diameter circular window of the test chamber. The time t was measured from the instant of the first appearance of hydrate crystals in the test chamber. (a) SDS added to c= 2000ppm, P = 3.93 ± 0.03 MPa, T = 275.0 (+1.8/-0.0) K, (b) SHS added to c= 40ppm, P = 3.91 ± 0.04 MPa, T = 275.0 (+1.8/-0.2) K. (Okutani et al. 2008)

However, all the previous morphological work done when surfactant is present in the system uses a camera or a video camera to capture and save images of hydrate formation (Figure 2.10). Although these images offer a visual observation of the system one may achieve a better understanding of hydrate formation by using a hydrate formation vessel suitable for morphological observations and equipped with a microscope which is attached to a camera in order to obtain magnified views. This will lead on to my research objectives.

## 2.3 Research Objectives

The objective of this study is to investigate the effect of three commercially available anionic surfactants (SDS, STS and SHS) on the morphology of methane/propane hydrate crystals growing at the interface of liquid/gas. The observed behaviour is compared to the behaviour in the absence of any chemical (pure water). The effect of sodium alkyl sulfates (C12) concentration and the degree of under-cooling are two variables the effect of which on the dynamics of hydrate growth is investigated. Besides the morphology, the effect of the surfactant on storage capacity of gas into hydrate, the ice – surfactant interaction, and the effect of surfactant injection during hydrate formation were also assessed.

# Chapter 3: EXPERIMENTAL APPARATUS AND PROCEDURES

## 3.1 Apparatus

The experimental set up is designed to study the morphology of hydrate formation/decomposition. Hydrate is formed inside crystallizer which consists of two main parts which are hollow, transparent polycarbonate (Lexan) column and stainless steel (SS) lids. This crystallizer is immersed into a temperature controlled water bath which was made of 10mm thick Plexiglas to allow visual observation from the outside (Figure 3.1).

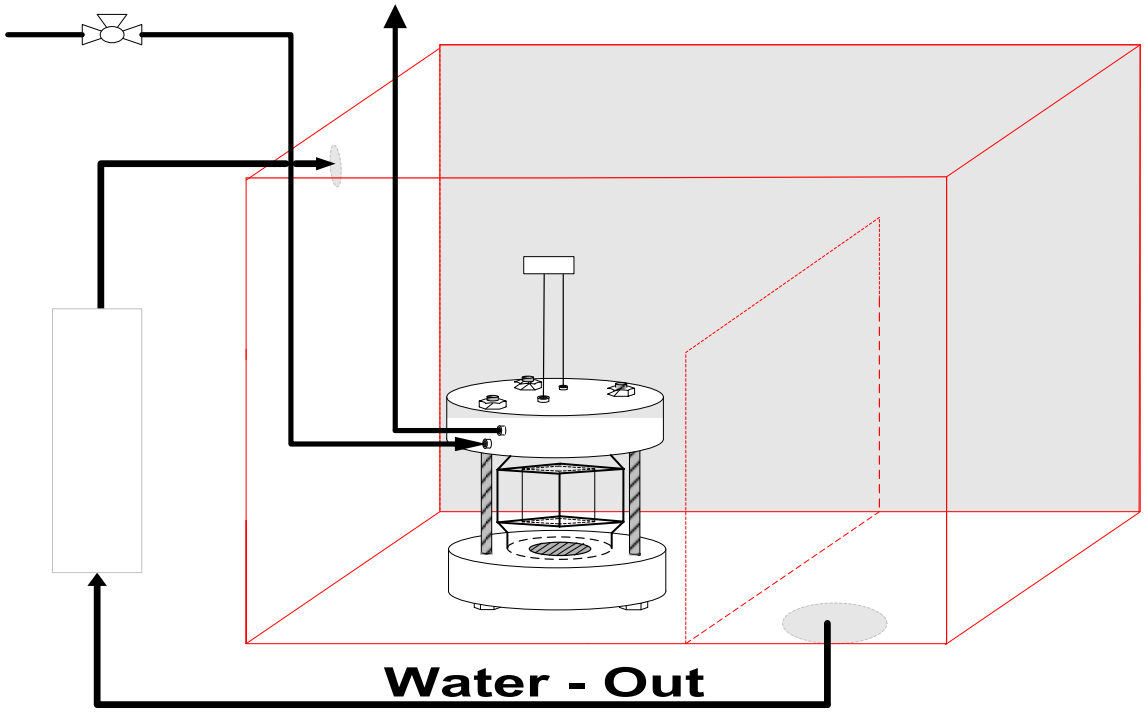


Figure 3.1: Water bath design to control temperature inside the crystallizer

The space to hold the fluids and hydrate crystals has top, middle and bottom portions that have the same vertical length of 25 mm but different horizontal cross sections as shown in Figure 3.2.

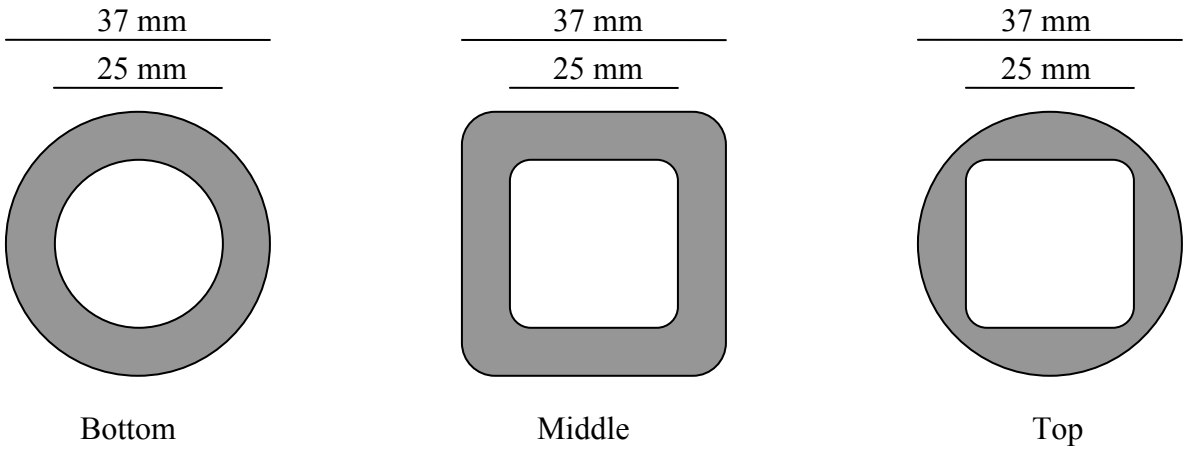


Figure 3.2: Dimensions of crystallizer middle portion

The top and bottom lids were stainless steel cylindrical plates with 44 mm in height and 114 mm in outer diameter. The actual pictures of the crystallizer can be seen in Figure 3.3. Two thermocouples were inserted, through port at the top of the lid, into the bulk of the liquid phase and the gas phase in order to monitor the temperature changes during hydrate formation/decomposition. The temperature of the crystallizer is controlled by two external heating/cooling systems. Two pressure gauges are installed on the line connected to the crystallizer. Data from both the thermocouples and pressure gauges are collected by the data acquisition system connected to a personal computer for analysis. A sampling valve is also located on the top lid of the crystallizer for collecting sample gas for analysis on a gas chromatograph (Varian, CP-3800). Stirring is possible since a magnetic stirrer is inserted

and placed at the bottom of the crystallizer. A schematic of the apparatus is given in Figure 3.4. Minor modification were made to the set up reported by Lee et al. (2006) by installing a digital pressure transmitter (Rosemount) coupled with a data acquisition system (National Instrument).

Figure 3.3: Actual pictures of crystallizer (top, middle, and bottom part)

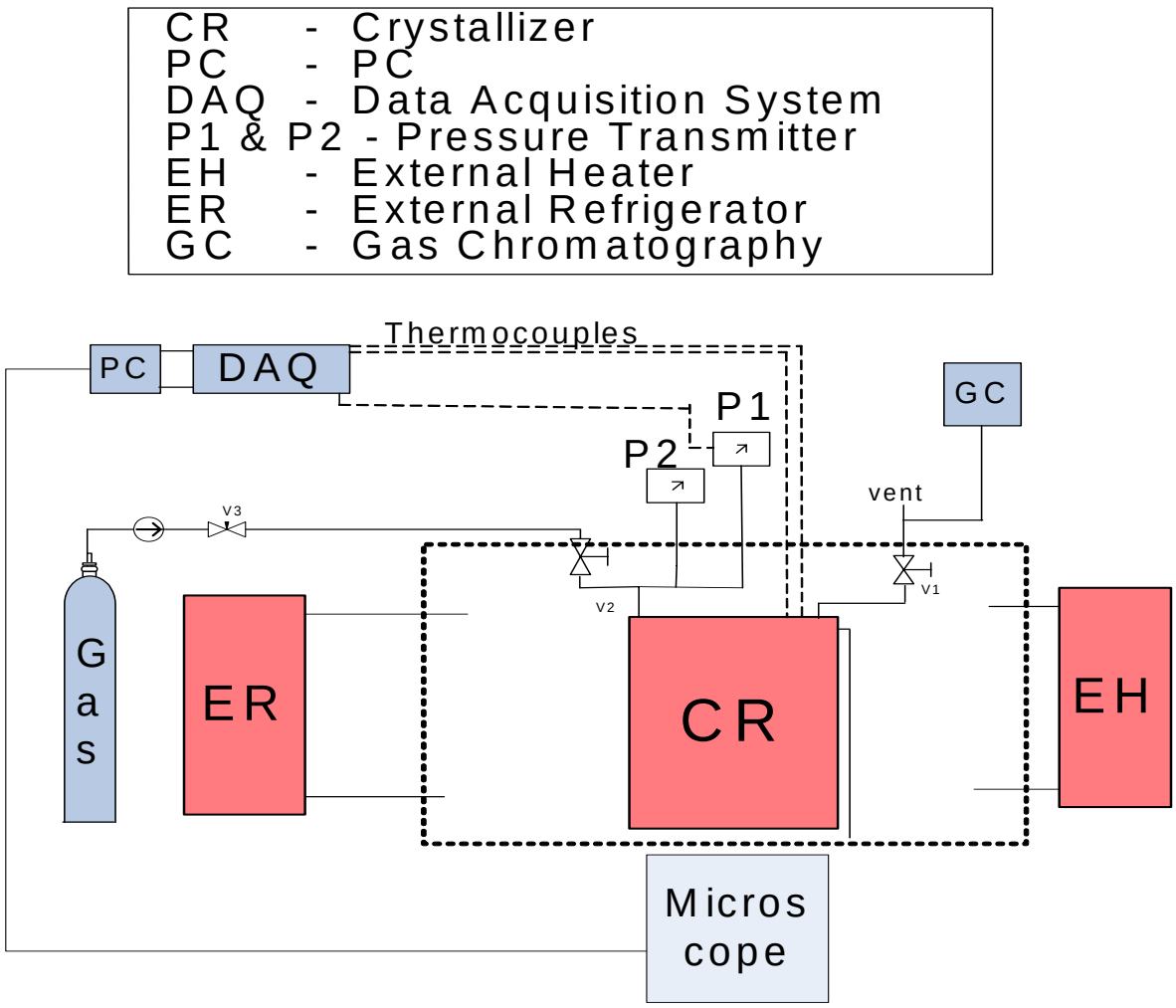


Figure 3.4: Schematic of apparatus (adapted from Lee et al. (2006) )

## 3.2 Materials

Materials used in the experiment were:

- Methane/propane gas with 90.5% methane and 9.5% propane composition from Praxair
- Distilled and de-ionized water
- Three commercially available surfactants:
    - Sodium Dodecyl Sulfate (SDS) ($C_{12}H_{25}SO_4Na$) with 99% purity from Sigma Aldrich
    - Sodium Tetradecyl Sulfate (STS) ($C_{14}H_{29}SO_4Na$) with 95% purity from Sigma Aldrich
    - Sodium N-Hexadecyl Sulfate (SHS) ($C_{16}H_{33}SO_4Na$) with 98% purity from Fisher Scientific
- Helium gas for Gas Chromatography analysis
- Nitrogen gas for Gas Chromatography analysis

### 3.2.1 Guest Gas for Hydrate Formation

The sample guest gas used to form hydrate was 90.5% Methane (C1) and 9.5% Propane (C3). This gas was obtained from Praxair. This composition was chosen in order to simulate natural gas light hydrocarbons; lower operating conditions, and simplifies morphology observation due to pure structure II hydrates formed. Exactly the same gas mixture has been used for other experiments with the same apparatus to test the morphology of hydrate formation (Kumar et al., 2007; Lee et al., 2006).

### 3.2.2 De-ionized Water

De-ionized water was used to avoid the contamination of unwanted metal ions that might affect the hydrate formation mechanism. De-ionized water is used to prepare the solution (liquids) for hydrate formation experiment. De-ionized water is also used to rinse the crystallizer after washing it.

### 3.2.3 Surfactant Used

There are three commercially available surfactant used in this paper which are Sodium Dodecyl Sulfate (SDS), Sodium Tetradecyl Sulfate (SHS), and Sodium Hexadecyl Sulfate (STS). Sodium dodecyl sulfate (SDS) (C12H25SO4Na) is an anionic surfactant that is used in industrial products including toothpastes, shampoos, shaving foams for its thickening effect and its ability to create lather. The molecule has a tail of 12 carbon atoms, attached to a sulfate group (Figure 3.5). The main difference between SDS, SHS, and STS is that the alkyl chain length where SDS has a tail of 12 carbon, STS has a tail of 14 carbon and SHS has a tail of 16 carbon atoms.


Figure 3.5: Sodium Dodecyl Sulfate (SDS) structure (C12)


Figure 3.6: Sodium Tetradecyl Sulfate (STS) structure (C14)


Figure 3.7: Sodium Hexadecyl Sulfate (SHS) structure (C16)

## 3.3 Equipment

The equipment used in this work were:

- Nikon D40 attached to Nikon SMZ- 2T for taking the system dimensions picture
- CCD camera (Sony, DXC 390) attached to a Nikon SMZ 1000 for taking more magnified view
- Water purifier (ELGA UHQ II, Great Britain) for producing de-ionized water
- Weighing Balance (Ohaus) accurate to 0.1mg
- Pipette accurate to 0.1 mL (Pipetteman)
- WinTV PVR2 for connecting CCD camera image to computer
- Magnetic Stirrer (Cimarec) for agitating solution inside the reactor
- Data acquisition system from National Instrument
- Digital Pressure Transmitter (Rosemont)
- Digital Pressure Indicator (HEISE)
- Logitech Web camera for taking timely image of temperature and pressure
- Water baths (Cole-Palmer and VWR) to maintain the temperature of the system
- Illuminator (Fiber lite – MI-150) source of light for microscope

- Weighing boats, Spatula, 100mL, 500mL, and 1000mL beakers / Erlenmeyer flasks for preparing solution
- Gas Chromatograph (Varian, CP-3800)
- Jefri High Pressure Positive Displacement Pump (DB Robinson Design & Manufacturing).

The picture of water purifier to produce de-ionized water (Figure 3.8), weighing balance (Figure 3.9), water baths to control the temperature of the experiments (Figure 3.10), illuminator (Figure 3.11) and gas chromatography to check the gas composition (Figure 3.12) are shown below.


Figure 3.8: Water purifier ELGA UHQ II

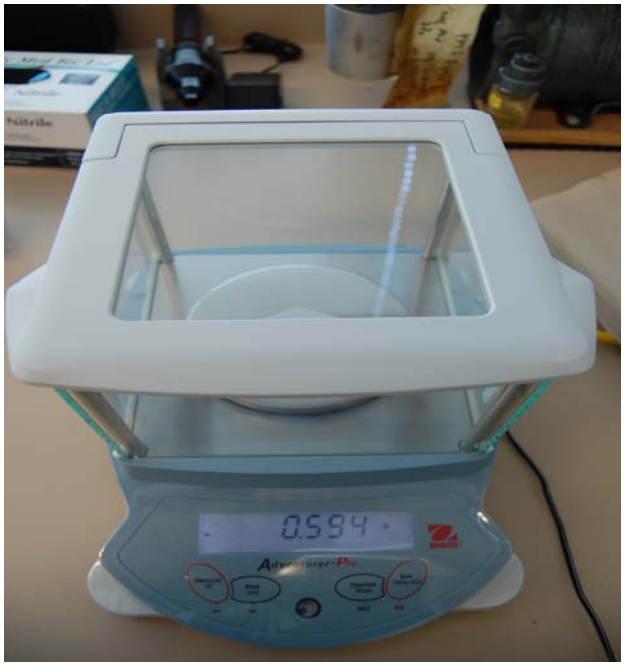


Figure 3.9: Weighing balance Ohaus


Figure 3.10: Water baths to control the temperature of crystallizer (VWR and Cole Palmer)

Figure 3.11:  Fiber-lite illuminator MI-150

Figure 3.12: Gas chromatography Varian CP-3800

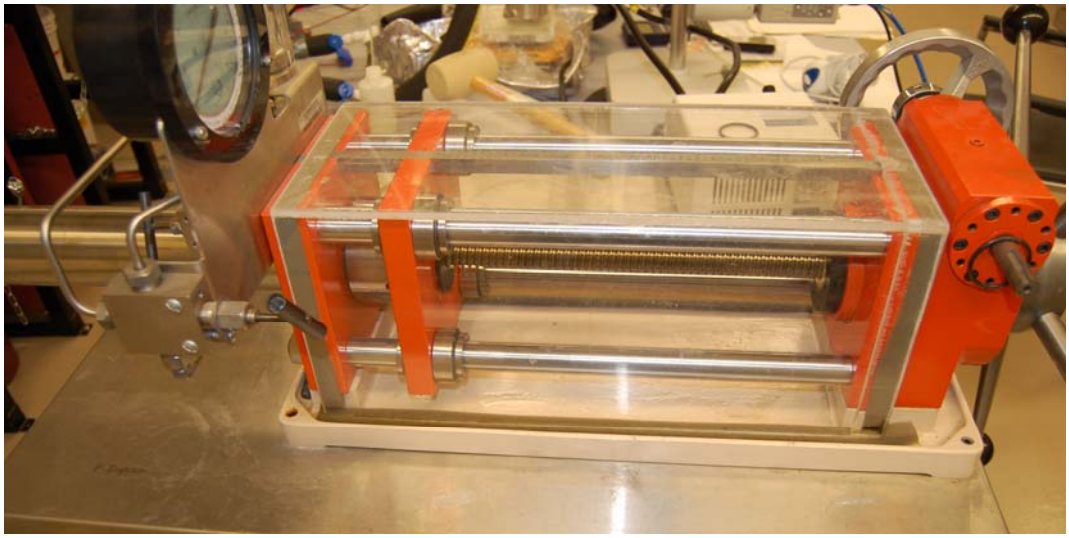

Figure 3.13: Jefri high pressure positive displacement pump

### 3.3.1 Microscopes for capturing images

Two microscopes were used during the experiments where each of them has a different purpose. Nikon SMZ-2T with Nikon D-40 attached was used to capture the system dimension images so that overall mechanism of hydrate formation can be studied (Figure 3.14). The lens used was 0.5x auxiliary lens.

Figure 3.14: Nikon SMZ 2T

The second microscope which is a Nikon SMZ 1000 was used to observe magnified images of hydrate crystals during hydrate formation (Figure 3.15). These images were saved to the computer with help of CCD camera (Sony, DXC 390). The lens used was P Plan APO 1x objectives lens. The CCD camera was connected to the computer using Win TV PVR hardware and the images were saved using SnagIt software.

Figure 3.15: Nikon SMZ 1000 with Sony DXC -390 attached

## 3.4 Procedures

There are three main experimental procedures that will be discussed below which include the method to prepare surfactant solutions, method to prepare memory water, and methods to run the experiment. Besides that, procedures to do the contact angle measurement and the experimental matrix will also be discussed after.

### 3.4.1 Surfactant Solution Preparation

The appearance of all three surfactants tested in this paper is that of white crystalline powders with the possibility to become nuisance dust. Nuisance dust, or inert dust, can be defined as dust that contains less than 1% quartz. Because of its low content of silicates, nuisance dust has a long history of having little adverse effect on the lungs. Due to its possibility to become nuisance dust, it is better to perform the solution preparation inside the fume hood.

There are a few concentrations of surfactant chosen to be tested which are listed in Table 3.1. In one of the experiments, 500ml – of 2200ppm of SDS is needed. The concentration shows that 2.2 gram of SDS is needed for 1 kg or 1 liter of water. So, in order to prepare 500ml of 2200ppm of SDS, 1.1 gram of SDS need to be mixed with de-ionized water. Mixing is done by inserting a magnetic stirrer and usually mixed takes place for at least 2 hours at ~500rpm. In addition, a pipette was used to measure the amount of de-ionized used.

### 3.4.2 Memory Water Preparation

Memory water is water that has experienced hydrate formation. Memory water will make the induction time for the subsequent experiment shorter so that the experimental time will

be less. Memory water is prepared inside the crystallizer. The memory water preparation procedure is shown in part of figure 3.14 and described below:

1. Inject 25 ml of liquid solution (water + surfactant) into the test cell
2. Flush the test cell three times with hydrate forming gas to remove any residual air
3. Set the pressure inside the reactor according to the desired pressure
4. Mix for 30 minutes so that the liquid is saturated with the guest species
5. Decrease the temperature of the system to the desired formation temperature (depend on the degree of under-cooling) while agitate the liquid
6. After the system temperature is dropped, hydrate formation is initiated and allowed to grow for 1 hr at constant temperature
7. Increase the temperature to 3 degree above the equilibrium temperature. Typically 60-90 minutes are required for the complete dissociation (no hydrate particles can be seen).

### 3.4.3 Morphology Experiment Procedure

1. After memory water is prepared, wait for standby time (120 min) before starting the formation experiment.
2. During the standby time, prepare the microscope so that it will be ready for taking images.
3. Rapidly cool the temperature of the crystallizer to the desired temperature without introducing any agitation and start taking pictures
4. Experiment can be stopped after no further pressure drop can be seen or noticed

5. Decompose hydrate with mixing until no more hydrate can be seen visually observed (Approximately 60 min)
6. Wait for standby time (120 min)
7. Repeat steps 2-6 until desired result is obtained

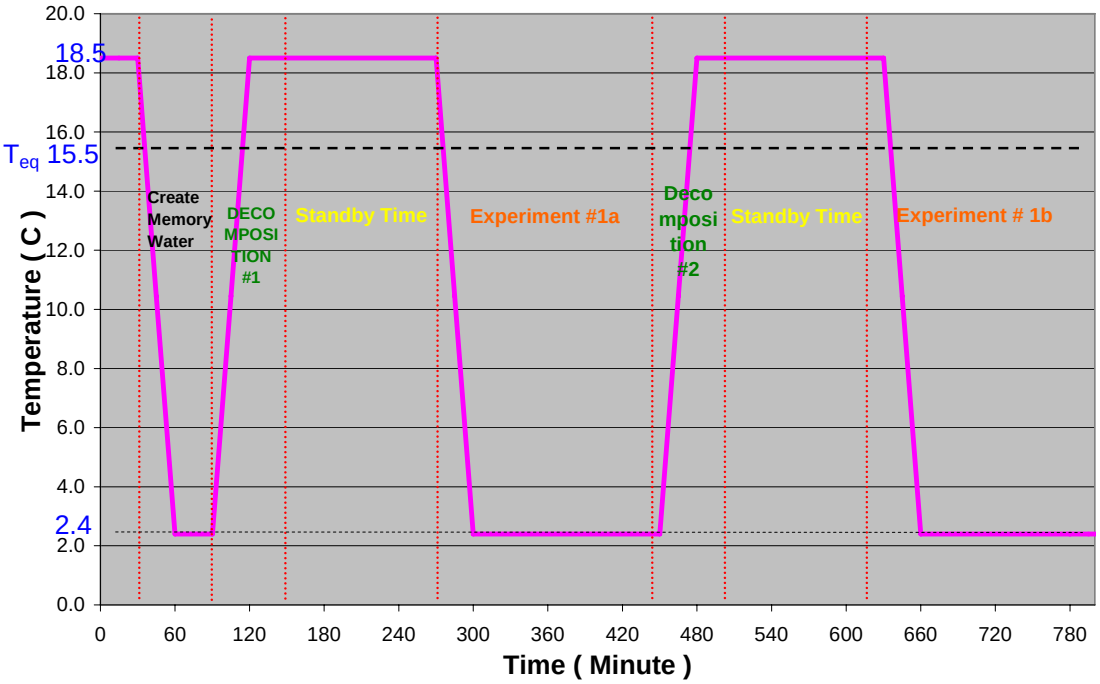


Figure 3.16: Experimental timeline for SDS 2200 ppm, 13.1$^{o}$C driving force, and 3200 kPa

### 3.4.4 Contact Angle Measurement Procedure

The purpose of this experiment is to test how much lower the contact angle is when surfactant is present in the system. This experiment was done on top of lexan surface which is the material used for making the transparent part in the crystallizer. The contact angle measurement procedure is described below:

1. Set timer on the camera to be 5 sec

2. Set the lighting so that there will be contrast between liquid droplet with solid surface
3. Dry the solid surface by blowing dry air
4. Pipette 1μl of liquid droplet into the edges of the solid surface (see **Figure 3.17**)

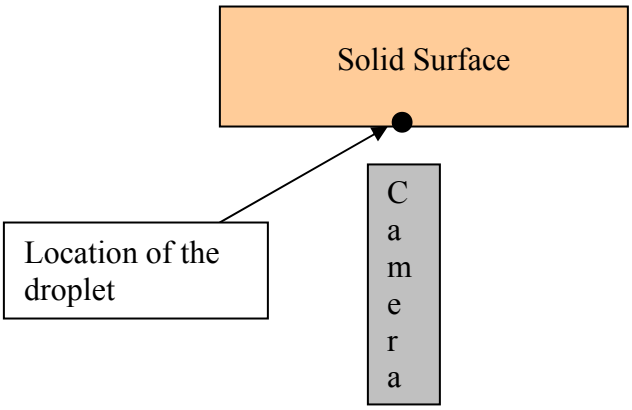


Figure 3.17: Location of liquid droplet on top of solid surface

5. Capture the image using camera
6. Use Fta32(Firsttenangstroms, VA, USA) software to determine the contact angle

### 3.4.5 Experimental Matrix for Morphology Experiments

There are three types of surfactant being tested which are sodium dodecyl sulfate (SDS), sodium tetradecyl sulfate (STS) and sodium hexadecyl sulfate (SHS). Three surfactants with different carbon alkyl chain length were chosen in order to study the effect of alkyl chain length. In this paper, the effects of different concentrations and different degrees of under-cooling on the morphology of methane-propane hydrate were also studied and SDS was chosen to be the surfactant tested for the study because it is commercially available and its properties are widely known. SDS surfactant concentrations of 2200, 645 and 242 ppm were chosen for the different concentration experiments. These three different concentration were chosen because 2200ppm is the concentration that gave the lowest surface tension (2005b),

the highest storage capacity (Lin et al., 2004) can be obtained when the concentration was 645ppm, and the critical micellar concentration (CMC) according to Zhong and Rogers (2000) was found to be 242 ppm. The concentrations of SHS and STS were chosen to be 300 and 40 ppm respectively since it gives the lowest surface tension (Watanabe et al., 2005b). The complete experimental matrix is summarized in the table shown below.

Table 3.1: Experimental matrix of this paper

| Experiment Number | Surfactant Conc. (ppm) | Pressure (kPa) | Temp Eq. ( C ) | Formation ( C ) | Delta T ( C ) | Pressure Drop (kPa) |
|---|---|---|---|---|---|---|
| A-1 | Water | 3200 | 15.5 | 2.4 | 13.1 | 58.5 |
| A-2 | Water | 3200 | 15.5 | 2.4 | 13.1 | 44.7 |
| B-1 | SDS-2200 | 3200 | 15.5 | 2.4 | 13.1 | 837.6 |
| B-2 | SDS-2200 | 3200 | 15.5 | 2.4 | 13.1 | 796.2 |
| B-3 | SDS-2200 | 3200 | 15.5 | 2.4 | 13.1 | 754.8 |
| C-1 | SDS-2200 | 2400 | 13.2 | 5.2 | 8 | 446.7 |
| C-2 | SDS-2200 | 2400 | 13.2 | 5.2 | 8 | 432.9 |
| C-3 | SDS-2200 | 2400 | 13.2 | 5.2 | 8 | 439.8 |
| D-1 | SDS-2200 | 1430 | 8.8 | 5.2 | 3.6 | 146.1 |
| D-2 | SDS-2200 | 1430 | 8.8 | 5.2 | 3.6 | 139.1 |
| D-3 | SDS-2200 | 1430 | 8.8 | 5.2 | 3.6 | 125.4 |
| E-1 | SDS-645 | 3200 | 15.5 | 2.4 | 13.1 | 830.6 |
| E-2 | SDS-645 | 3200 | 15.5 | 2.4 | 13.1 | 754.8 |
| E-3 | SDS-645 | 3200 | 15.5 | 2.4 | 13.1 | 734.1 |
| F-1 | SDS-242 | 3200 | 15.5 | 2.4 | 13.1 | 782.5 |
| F-2 | SDS-242 | 3200 | 15.5 | 2.4 | 13.1 | 754.8 |
| F-3 | SDS-242 | 3200 | 15.5 | 2.4 | 13.1 | 637.6 |
| G-1 | STS-300 | 3200 | 15.5 | 2.4 | 13.1 | 823.8 |
| G-2 | STS-300 | 3200 | 15.5 | 2.4 | 13.1 | 768.7 |
| G-3 | STS-300 | 3200 | 15.5 | 2.4 | 13.1 | 706.5 |
| H-1 | SHS-40 | 3200 | 15.5 | 2.4 | 13.1 | 775.5 |
| H-2 | SHS-40 | 3200 | 15.5 | 2.4 | 13.1 | 699.6 |
| H-3 | SHS-40 | 3200 | 15.5 | 2.4 | 13.1 | 678.9 |

## 3.5 Procedure of Ice-Surfactant Interaction Experiment

Two sets of SDS solution with concentration of 1000ppm and 2000ppm were prepared in order to test the interaction between an ice surface and the surfactant. 10ml of SDS solution was put in a beaker and 4ml of ice in a half-sphere shape with a diameter of approximately 22mm was also prepared in order to be dipped inside the SDS solution.

This experiment was done inside a cold room with a temperature around $4^{o}$C in order to minimize melting of ice during the experiment. The contact angle of 1000ppm, 2000ppm of SDS solution before and after experiment was measured using FTA32 software made by Firsttenangstroms, USA. Besides that, contact angle of water and water from melted ice after the experiment were also measured. All of the contact angle measurement was done on Ultra High Molecular Weight Polyethylene surface. The procedure followed in this experiment was the same as the contact angle measurement for morphology experiment.

## 3.6 Modification and Procedure of High Pressure Injection of Surfactant Solution Experiment

Some modification has been made to the morphology apparatus so that injection of liquid through the bottom of crystallizer during hydrate formation is possible. The modification can be seen in Figure 3.18.

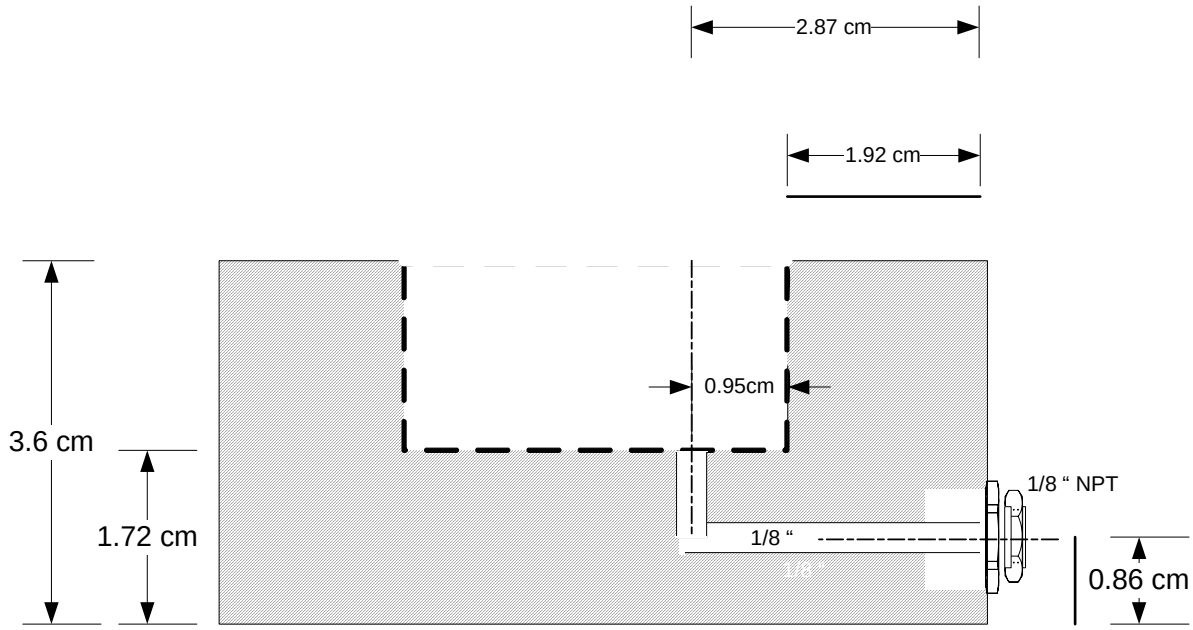


Figure 3.18: Modification to morphology apparatus to allow liquid injection from the bottom of the crystallizer

The procedure followed in this experiment is exactly the same as the formation experiment done before and the difference is that 1ml of SDS solution is injected after a thin liquid film is formed at the gas liquid interface. It is noted that once the surfactant solution was injected the resultant concentration of SDS was 2200ppm. The experimental matrix of the high pressure injection of surfactant solution experiment is shown in Table 3.2 .

Table 3.2: Experimental matrix for high pressure injection of surfactant solution experiment

| Experiment Number | Surfactant Conc. (ppm) | Pressure (kPa) | Temp Eq. ( C ) | Formation ( C ) | Delta T ( C ) |
|---|---|---|---|---|---|
| Dynamic 1 | Water | 3200 | 15.5 | 2.4 | 13.1 |
| Dynamic 2 | Water | 3200 | 15.5 | 2.4 | 13.1 |

# Chapter 4: RESULTS AND DISCUSSION

Results of the morphology studies with and without surfactant are presented first. Morphology is concerned with the observation of shapes and sizes of the hydrate phase formation boundaries, but whose length scales are much larger than molecular structure and much smaller than system dimension. In most of the experiments, the area being observed is the gas-liquid interface which can be seen in Figure 4.1.The experimental conditions, surfactant concentration and type of surfactant are summarized in table 3.1. The effect of surfactant on the storage capacity according to gas uptake measurements is discussed next. The total pressure drop during an experiment is also reported in table 3.1. The pressure drop indicates the amount of gas consumed for hydrate crystal formation so that a higher pressure drop means a higher conversion of water into hydrate

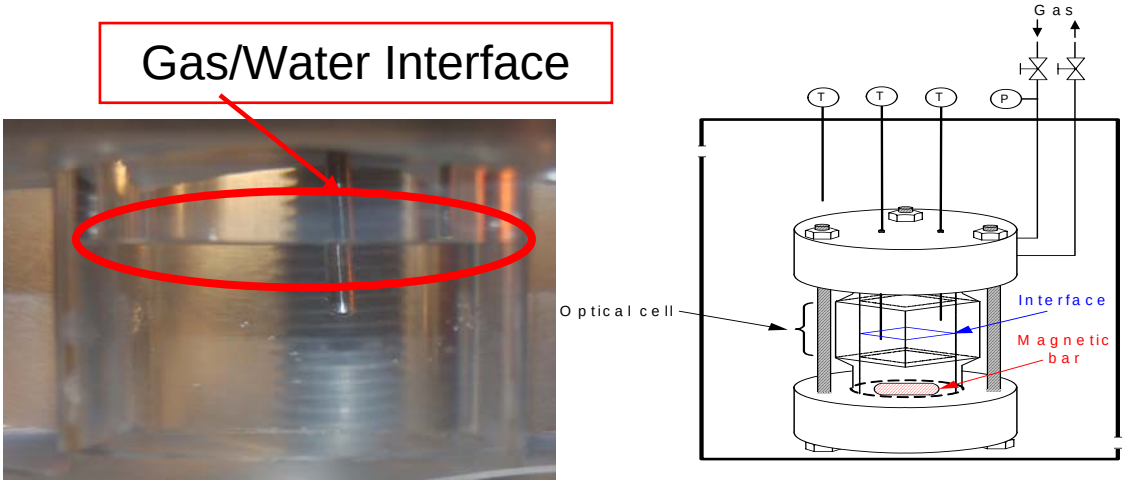


Figure 4.1: Part of the apparatus showing the observed gas/water interface during hydrate formation

## 4.1 Morphology of Methane-Propane Hydrate Crystals without Surfactant Additives

This experiment was conducted in order to compare the results with those obtained by Lee et al. (2006). Without additive in the system, hydrates started to grow at the gas/water interface as a thin film and covered the entire gas/ water interface within30 s. Then, needle-like hydrate crystals were observed to grow downward from the thin film into the bulk water. These crystals later grew as dendrites; Figure 4.2 shows sequential images of hydrate growth. The observed crystal growth morphology is in agreement with that reported by Lee at al. (2006).

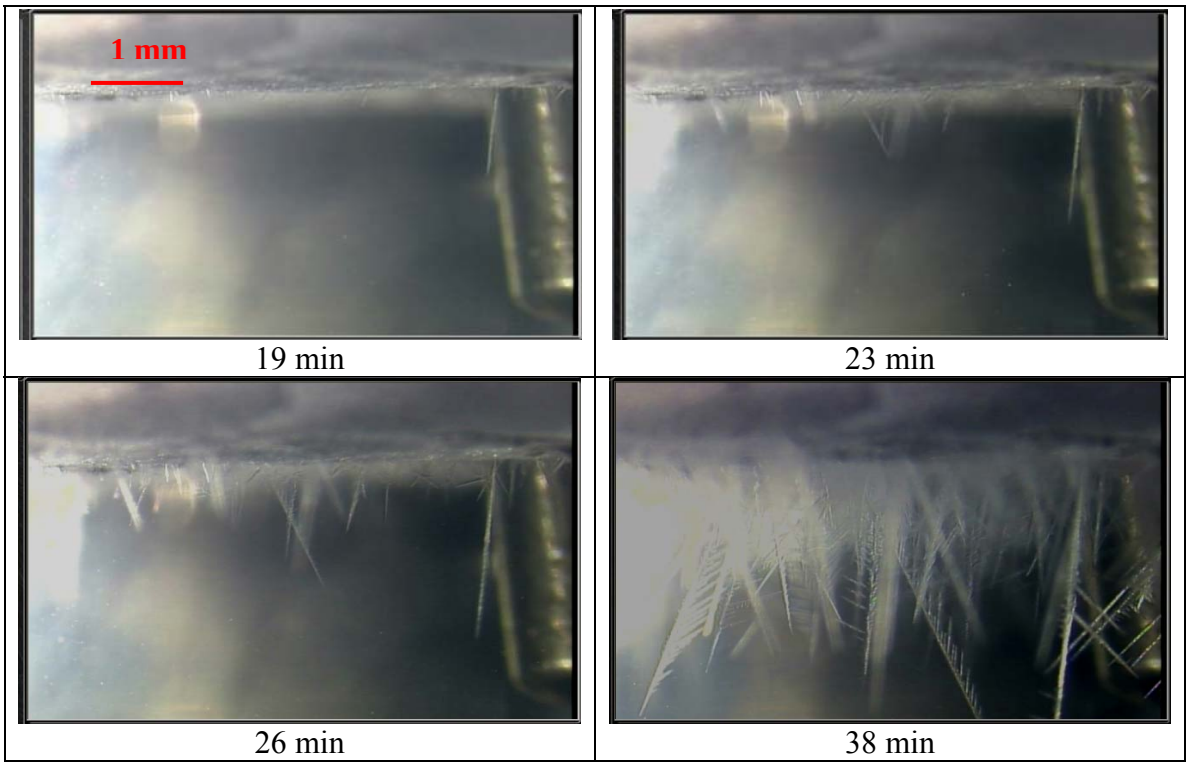


Figure 4.2: Sequential images of methane-propane hydrate crystals formation at 3200 kPa, T = 275.5K and ΔT=13.1o under-cooling (Experiment A). The time lapse after the formation is indicated below each image

.

## 4.2 Morphology of Methane-Propane Hydrate Crystals in the Presence of Surfactants

### 4.2.1 General Observations

It was observed that when any three of the surfactants is present in the system (Figure 4.3), hydrate crystals were first seen in the vicinity of the water/gas/solid line or at the tip of the thermocouple touching the water surface (Figure 4.4). This work reports for the first time the location where hydrate formation started in a surfactant containing system. On the other hand, in the absence of any additive, hydrates appear as a thin film at the gas/water interface as observed in Figure 4.2 and also reported in the literature (Lee et al., 2006).

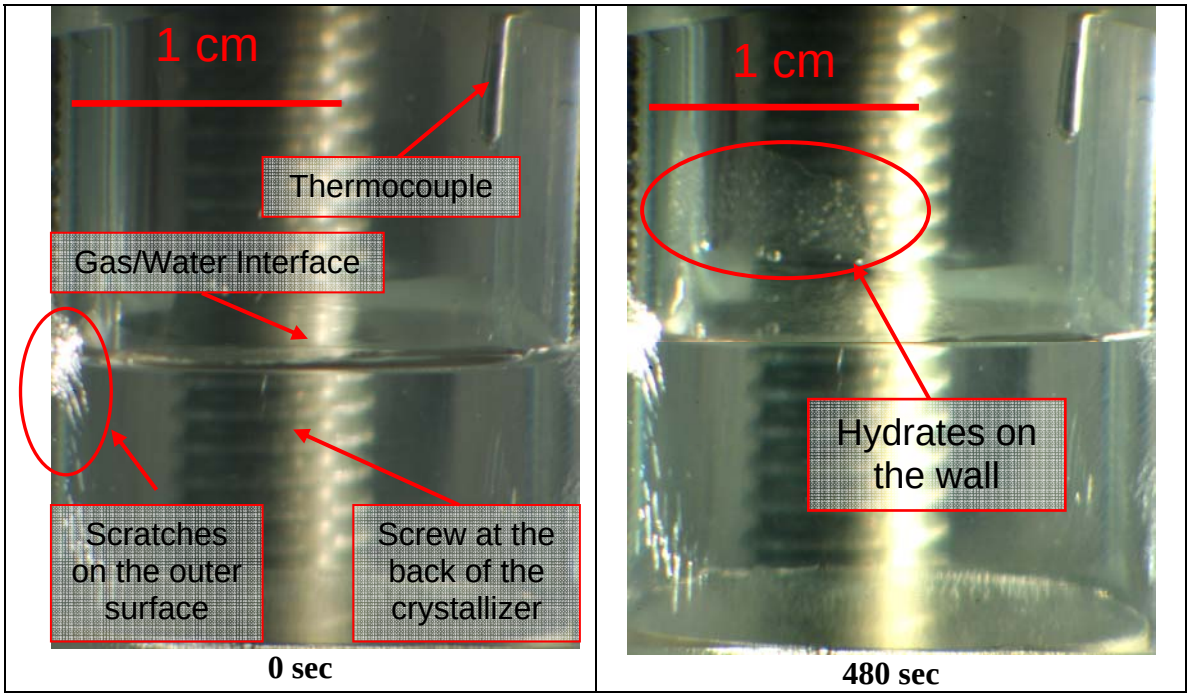


Figure 4.3: First growth of hydrate crystals at $\Delta T = 13.1^{o}C$, (Experiment G-3), and without thermocouple present in the liquid phase. The time lapse after the formation started is indicated below each image.

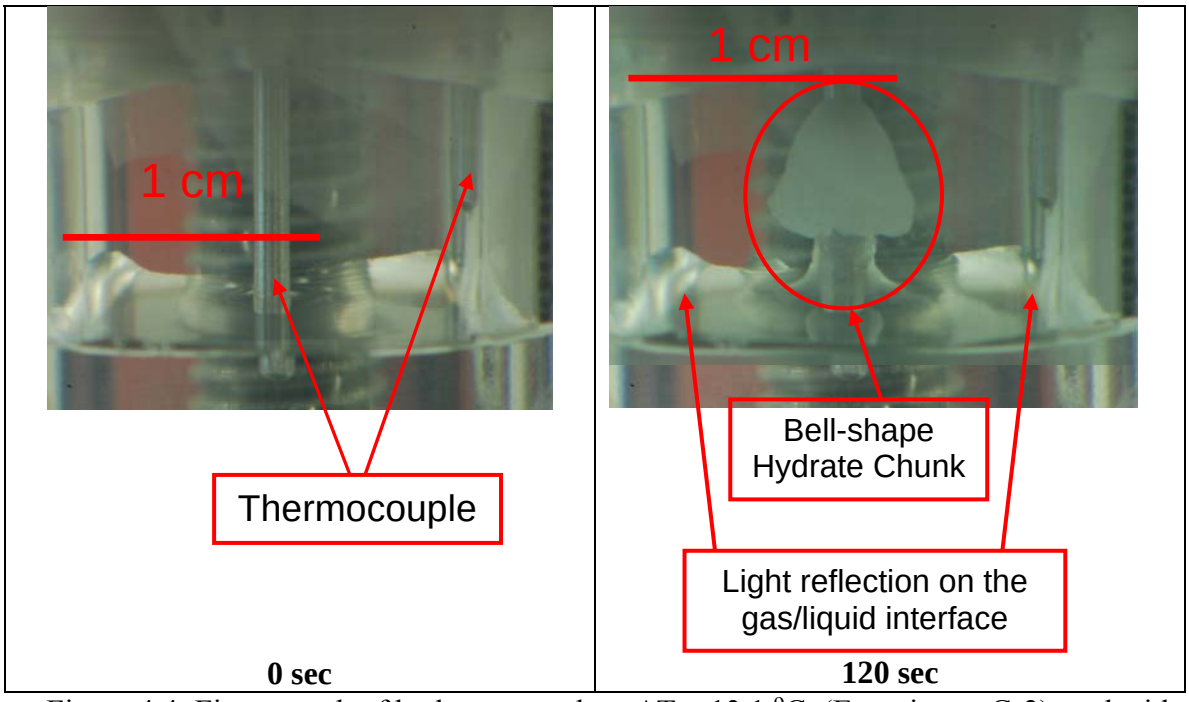


Figure 4.4: First growth of hydrate crystals at $\Delta T = 13.1\ ^{o}C$, (Experiment G-2), and with thermocouple present in the liquid phase. The time lapse after the formation started is indicated below each image.

As mentioned before the addition of the surfactant decreases the surface tension of water and lowers the contact angle. The contact angle on the Lexan surface (crystallizer material) was determined experimentally using FTA32 software (Firsttenangstroms, VA, USA). As seen in Figure 4.5 addition of SDS 2200ppm decreases the contact angle by about $11^{o}$. The contact angle was measured using Fta32 software and Figure 4.6 shows a schematic of the gas/water interface with and without surfactant. Due to lowering of the contact angle with the surfactant a film-like interface is created along the wall and below the gas/water/solid line. It is interesting that this liquid becomes the preferred location for nucleation and initiation of hydrate growth.

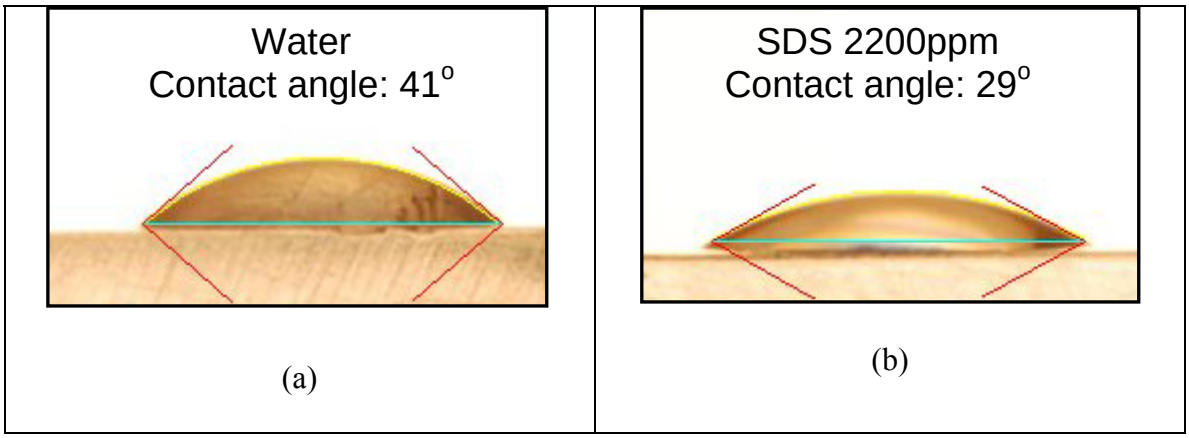


Figure 4.5: Contact angle measurement using droplet of solution on the lexan surface

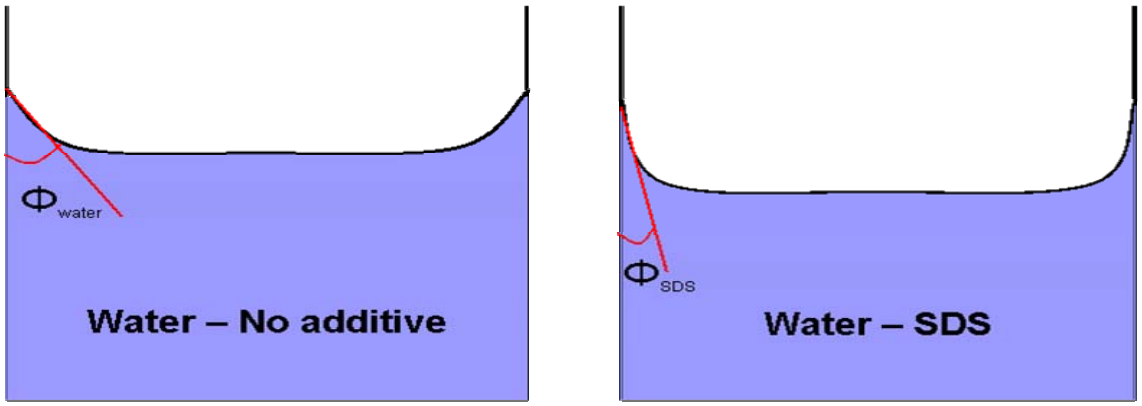


Figure 4.6: Contact angle comparison of system without additives (a) and with SDS surfactant (concentration 2200ppm) (b)

In Figure 4.4, hydrates can be seen to start growing along the thermocouple circumference of the thermocouple part that is located just above the liquid solution but no hydrates can be seen to grow on the crystallizer wall yet. However, in Figure 4.3 hydrates started to grow on the crystallizer wall. This phenomenon confirms that the stainless steel (thermocouple)/water interface is a more preferred location for hydrate nucleation compared to the crystallizer wall made from Lexan. Perhaps this is due to the fact that the metal surface is a more effective material for heat removal or a preferred site for heterogeneous nucleation.

In addition, the image on the right from Figure 4.4 also shows a bell-shaped hydrate crystal chunk to grow along the thermocouple body above the liquid solution. The bell-shaped hydrate chunk indicates that hydrate growth on the thermocouple is not only vertical (upward) but also horizontal (the chunk gets thicker). The image shown in Figure 4.4 may be compared to that given in Fig. 6 in the paper of Gayet et al. (2005). Gayet et al. (2005) used a $10^{-3}$ wt% SDS solution and propane at 0.4MPa and 274K.

The magnified images of the thermocouple body during hydrate formation are also shown in Figure 4.7 to give a better illustration of the growth of the hydrate crystal chunk. These series of images show that bulky hydrate layer started to form at the water/gas/thermocouple line and then grew upward at a rate faster than its growth to the sides. The focus of these images is ~1-2 mm above the gas/water interface and the time corresponding to the images is indicated below each image.

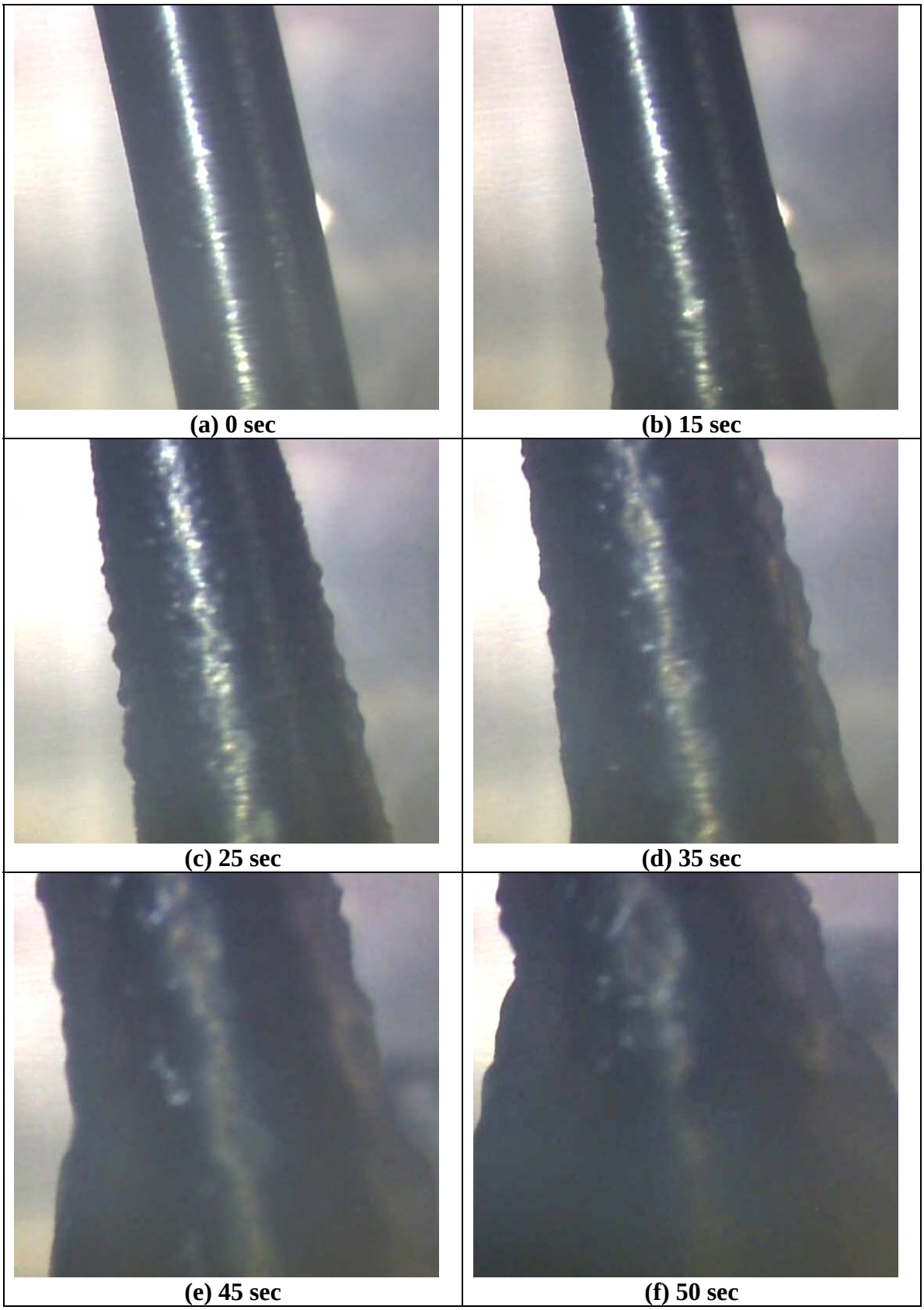

**(a) 0 sec** **(b) 15 sec**

**(c) 25 sec** **(d) 35 sec**

**(e) 45 sec** **(f) 50 sec**

Figure 4.7: Hydrate growth on thermocouple body (Experiment G-2)

Following nucleation, hydrate was also seen to grow radially to cover the gas/liquid water interface, not with a hydrate film but with "mushy" hydrate crystals as seen in Figure 4.8. The mushy hydrate crystals on the gas/liquid water interface were initiated from the base of the hydrate chunk on the thermocouple body and grew to cover the entire gas/liquid water interface.

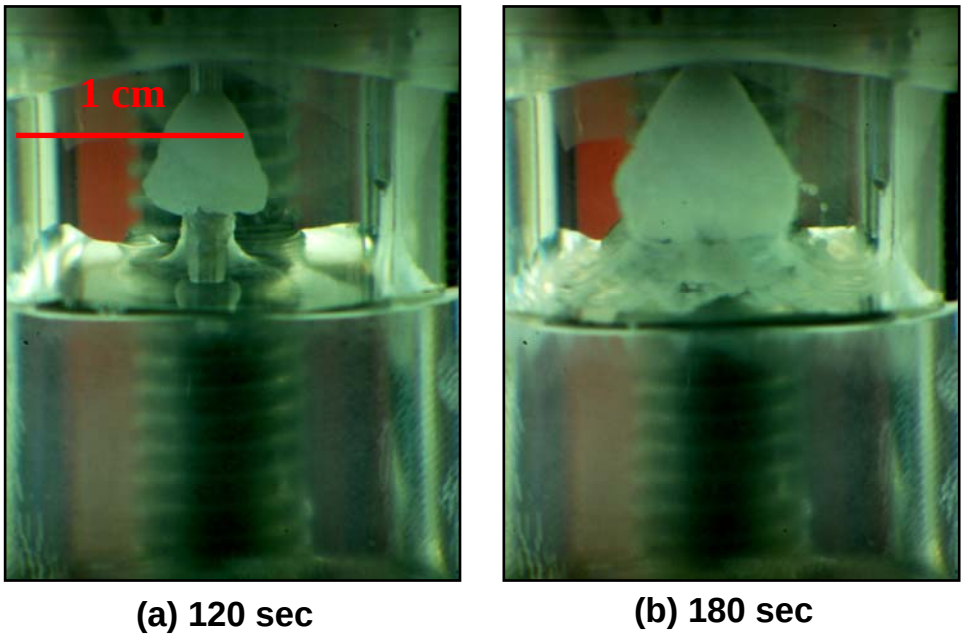


Figure 4.8: Mushy hydrate growth in the gas/water interface (Experiment G-2)

In addition, as shown in Figure 4.9, branches of fibre-like crystal were seen to grow towards the bulk water phase, unlike the system without any surfactant where only dendritic crystals were seen. The diameter of each fibre shown in the figure below is approximately 1 – 2 μm. These fibre-like crystals were seen to grow when mushy hydrate crystals were also growing to cover the entire water/gas interface.

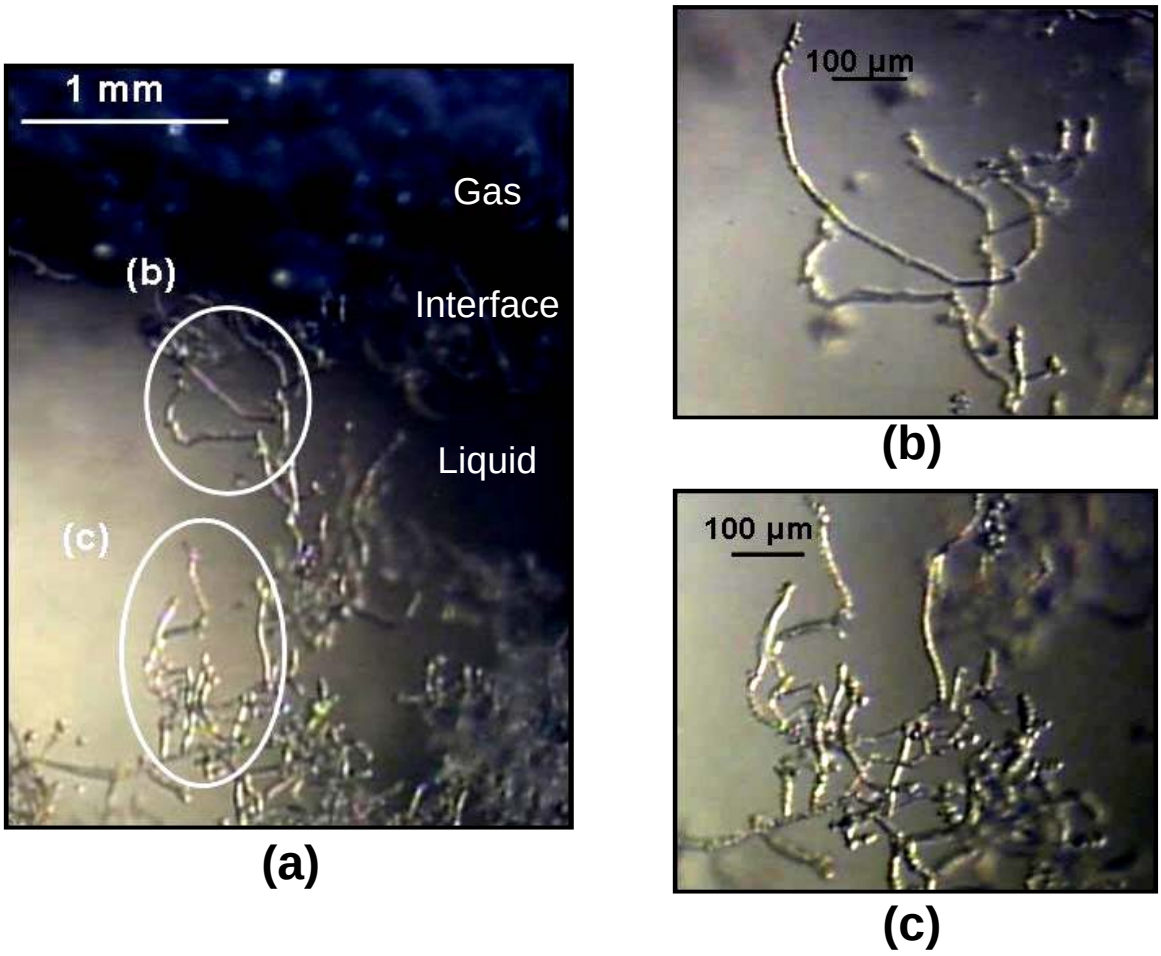


Figure 4.9: Images of hydrate crystal during hydrate formation with surfactant present in the system (Experiment C-1). Image (b) and (c) are magnified images from (a).

After forming mushy hydrate layer on the water/gas interface and fibre-like crystal below it, bulky hydrate layers on the wall continued to grow upward. Besides hydrate growth on the crystallizer wall, mushy hydrates on the liquid-gas interface also grew thicker towards the bulk water. At the end of the experiment, it was found that about 22.8 to 23ml of aqueous liquid solution was still left in the crystallizer. The total amount of water consumed was estimated by assuming a hydration number equal to 8. For calculating the hydration number, we estimated the occupancies of the small and large cages by methane/propane molecules

on the basis of CSMHYD (Sloan, 1998). The observations discussed so far are also valid for SDS and SHS provided that the driving force/degree of under-cooling is the same (Experiment B, E, F, G and H).

It should be noted that due to water consumption, the surfactant concentration increased and the final concentration of surfactant in all of the experiments is summarized in Table 4.1 shown below. However, this assumes that surfactant was not attached (adsorbed) to the hydrate surface. In order to test this assumption, two experiments were done to test the SDS surfactant concentration left after hydrate formation. These two experiments were done with experimental condition the same as experiment B where the starting SDS surfactant concentration is 2200ppm. It was found that the contact angle of the liquid after hydrate formation to be slightly higher which means the surfactants do attached on the hydrate surface. The result is tabulated in table 4.2.

Zhang et al. reported the solubility of SDS near the methane hydrate forming conditions which is shown in Figure 4.10 below. Based on this finding, Zhang et al. (2007) reported that under hydrate forming conditions, SDS molecules added to water in excess of 1780ppm, should form solid surfactant crystals. Since SDS concentration in experiment B, C and D was 2200ppm; solid crystal would form instead of micelles. However, such crystals were not seen. Although the final SDS surfactant concentration is above the CMC (Table 4.3), micelles do not form because the experimental temperature is below the krafft point (Table 4.4). Figure 4.11 shows a surfactant/water phase diagram, the solubility and CMC curves.

Table 4.1: Surfactant Final Concentration

| Exp. | Surfactant | | | $P_{exp}$ | $T_{exp}$ | Pressure Drop |
|---|---|---|---|---|---|---|
| | Type | Initial Concentration | Expected Final Concentration | | | |
| Number | | (ppm) | (ppm) | (kPa) | ( C ) | (kPa) |
| A-1 | Water | - | | 3200 | 2.4 | 58.5 |
| A-2 | Water | - | | 3200 | 2.4 | 44.7 |
| B-1 | SDS | 2200 | 2376 | 3200 | 2.4 | 837.6 |
| B-2 | SDS | 2200 | 2366 | 3200 | 2.4 | 796.2 |
| B-3 | SDS | 2200 | 2357 | 3200 | 2.4 | 754.8 |
| C-1 | SDS | 2200 | 2291 | 2400 | 5.2 | 446.7 |
| C-2 | SDS | 2200 | 2289 | 2400 | 5.2 | 432.9 |
| C-3 | SDS | 2200 | 2290 | 2400 | 5.2 | 439.8 |
| D-1 | SDS | 2200 | 2229 | 1430 | 5.2 | 146.1 |
| D-2 | SDS | 2200 | 2228 | 1430 | 5.2 | 139.1 |
| D-3 | SDS | 2200 | 2225 | 1430 | 5.2 | 125.4 |
| E-1 | SDS | 645 | 696 | 3200 | 2.4 | 830.6 |
| E-2 | SDS | 645 | 691 | 3200 | 2.4 | 754.8 |
| E-3 | SDS | 645 | 690 | 3200 | 2.4 | 734.1 |
| F-1 | SDS | 242 | 260 | 3200 | 2.4 | 782.5 |
| F-2 | SDS | 242 | 259 | 3200 | 2.4 | 754.8 |
| F-3 | SDS | 242 | 257 | 3200 | 2.4 | 637.6 |
| G-1 | STS | 300 | 324 | 3200 | 2.4 | 823.8 |
| G-2 | STS | 300 | 322 | 3200 | 2.4 | 768.7 |
| G-3 | STS | 300 | 320 | 3200 | 2.4 | 706.5 |
| H-1 | SHS | 40 | 42.9 | 3200 | 2.4 | 775.5 |
| H-2 | SHS | 40 | 42.6 | 3200 | 2.4 | 699.6 |
| H-3 | SHS | 40 | 42.6 | 3200 | 2.4 | 678.9 |

Table 4.2: Contact angle measurement of liquid after hydrate formation with SDS present in the systems (Initial SDS concentration = 2200ppm)

| | Contact Angle | |
|---|---|---|
| | Initial SDS concentration which is 2200ppm | Final SDS concentration after hydrate formation |
| **Exp. 1** | 45.80 | 45.36 |
| **Exp. 2** | 45.58 | 46.82 |
| **average** | 45.69 | 46.09 |

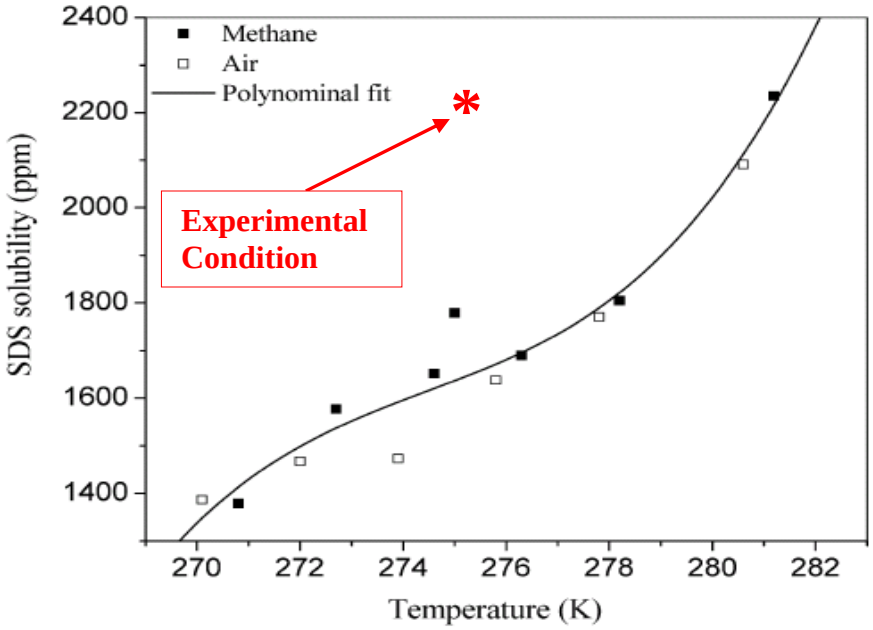


Figure 4.10: SDS solubility in liquid water near methane hydrate-forming conditions (the $P_{exp}/P_{diss}$ ratio ranges from 1.0 to 1.7) and under atmospheric pressure (Zhang et al. 2007)

Table 4.3: Critical Micelle Concentration (CMC) of SDS in water

| Data Source | Temperature | CMC (ppm) |
|---|---|---|
| Flockhart (1961) | 10.5°C | 2490 |
| | 14.1°C | 2440 |
| | 18°C | 2400 |
| | 25°C | 2350 |
| Zhong and Rogers (2000) | 3-5°C | 242 |
| | 25°C | 2725 |
| Rana et al. (2002) | 25°C | 2300 |
| Sun et al. (2004) | 0°C | ~500 |
| Di Profio et al. (2005) | 2°C | ~2300 |

Table 4.4: Krafft point for SDS, STS and SHS in water

| Surfactant | **Data Source** | **Krafft Point ($^oC$)** |
|---|---|---|
| SDS | Weil et al. (1963) | 16 |
| SDS | Nakayama and Shinoda (1967) | 12 |
| SDS | Lange and Schwuger (1968) | 8 |
| STS | Takeda et al. (1996) | 30 |
| SHS | Kong et al. (1987) | 36 |

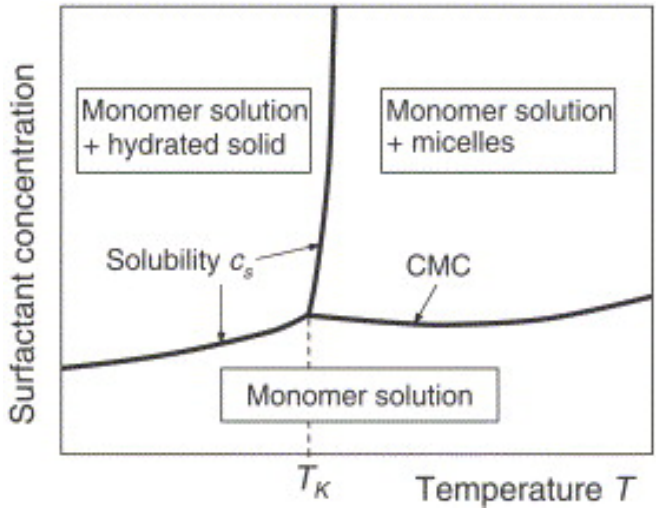


Figure 4.11: Phase diagram (schematic) for an ionic surfactant mixed in water Watanabe et al. (2005a)

Figure 4.12 and Figure 4.13 show two typical series of hydrate formation process using a 25 ml aqueous solution containing 300ppm of Sodium Tetradecyl Sulfate (STS). In Figure 4.12, no thermocouple in the liquid phase is installed. Figure 4.13 shows the macroscopic hydrate-phase growth when a thermocouple is present in the liquid phase. The sequences shown in Figure 4.12 and Figure 4.13 can be compared to that given in Figure 2 in the paper of Okutani et al. (2008) and Figure 4 in the paper of Watanabe et al. (2005a)

It is also noted from Figure 4.12 and Figure 4.13 that the hydrate layers along the crystallizer wall consist of fine fibre-like crystals (540 sec and 560 sec images from Figure 4.12, and 200 sec and 210 sec images from Figure 4.13). The bulky hydrate layer on the wall and/or thermocouple body falls into the liquid pool once it gets heavier and the water level decreases so that there is less support from the bottom. Once the bulky hydrate chunk drops back to the liquid pool, it leaves a wet surface on the wall that will quickly form hydrate again. In this apparatus, a hydrate layer will continue to grow until most of the free surface on the wall above the liquid level is covered.

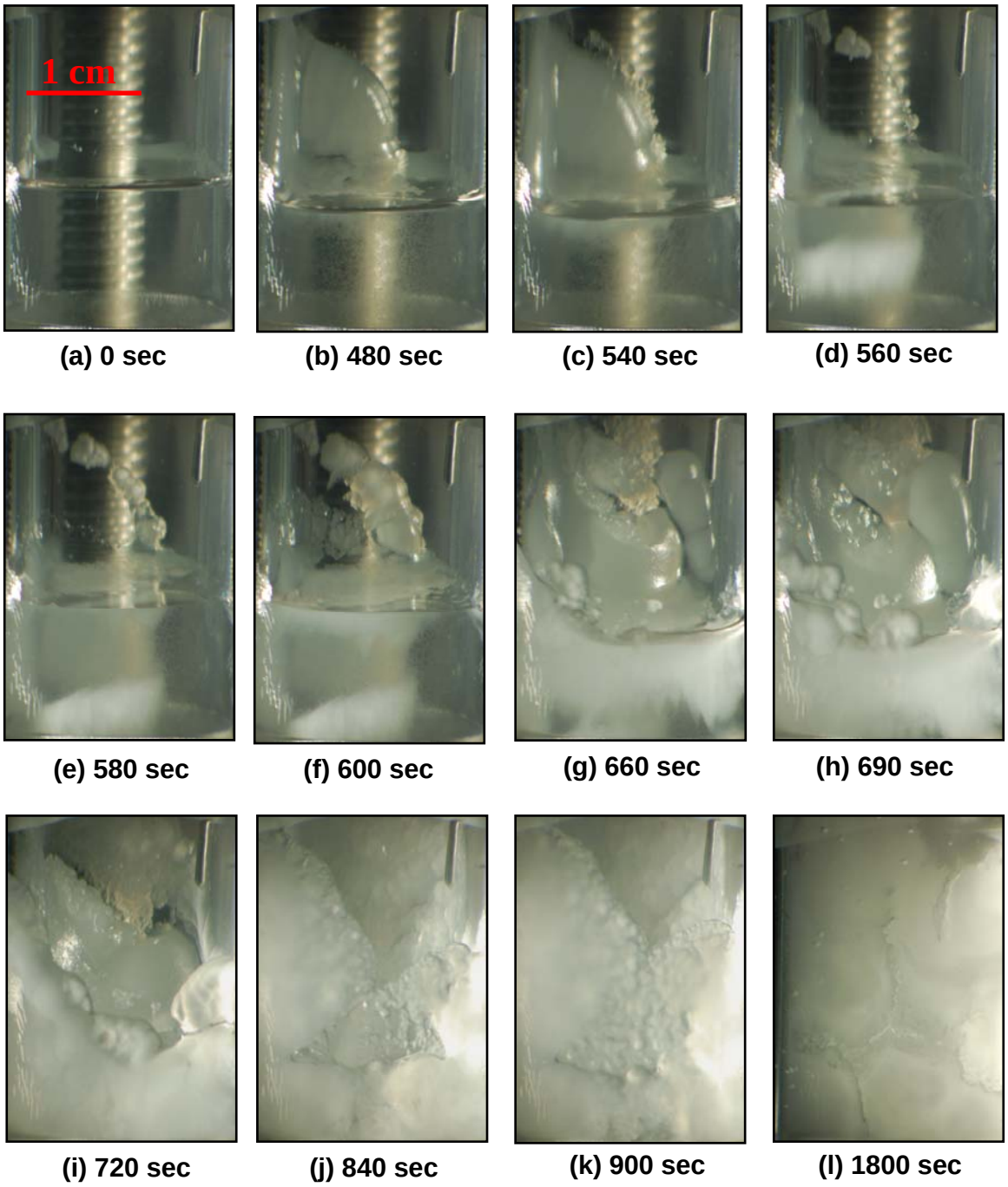


Figure 4.12: Sequential images of hydrate crystals from hydrate formation without thermocouple in the water phase (Experiment G-3)

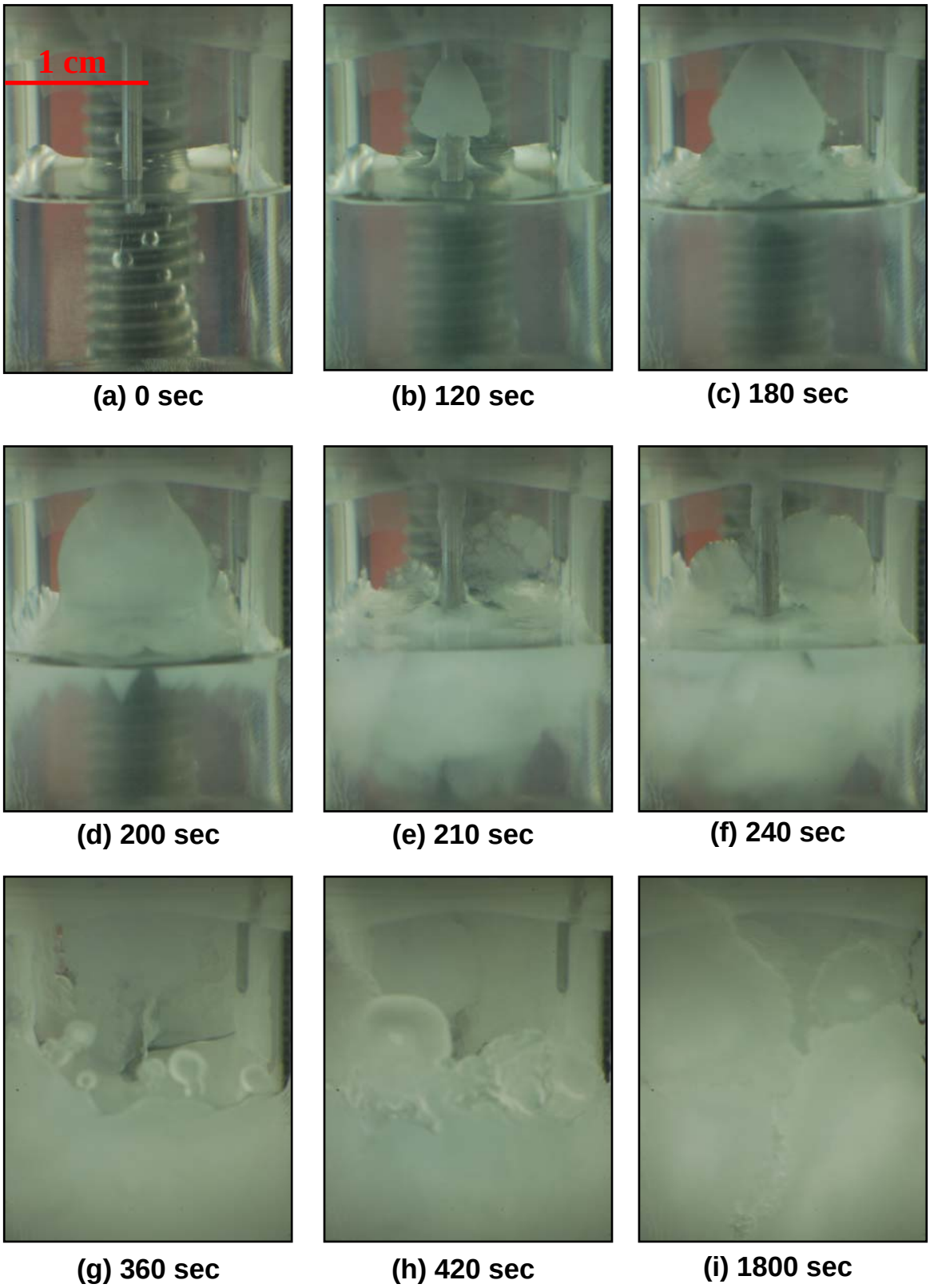


Figure 4.13: Sequential images of hydrate crystals from hydrate formation with thermocouple in the water phase (Experiment G-2)

In general, the behaviour of the macroscopic hydrate-phase growth observed here is in agreement with the descriptions given by Kutergin et al. (1992), Mel'nikov et al. (1998), Zhong and Rogers (2000), Watanabe et al. (2005a), Gayet et al. (2005), Pang et al. (2007) and Okutani et al. (2008). Despite the general similarity in the hydrate growth mechanism, some morphological differences between them are still noted. In comparison with the findings of Okutani et al. (2008) where they used methane as their guest gas species, we note several morphological differences with our work which used a mixture of methane/propane (90.5 – 9.5 mol%). The differences are stated below.

- It was found that branches of fibre-like crystal to grow instead of dendrites
- The "mushy" hydrate layer which grows downward from gas/liquid interface was composed of fine fibre like crystals instead of fine dendrites in the case of methane hydrate.
- There is a possibility that the hydrate layer which grows on the crystallizer also contains fine fibre-like crystals

### 4.2.2 Fibre-like Hydrate Crystal Growth in the Bulk Water

The growth of fibre like crystals in the bulk water can also be seen in Figure 4.14 where the red elliptical mark identifies the same crystal at the time indicated below each image. As seen, the red mark moves downwards in order to locate the same crystal because there is hydrate formation above it. The newly formed crystal is identified in Figure 4.14d by a rectangle.

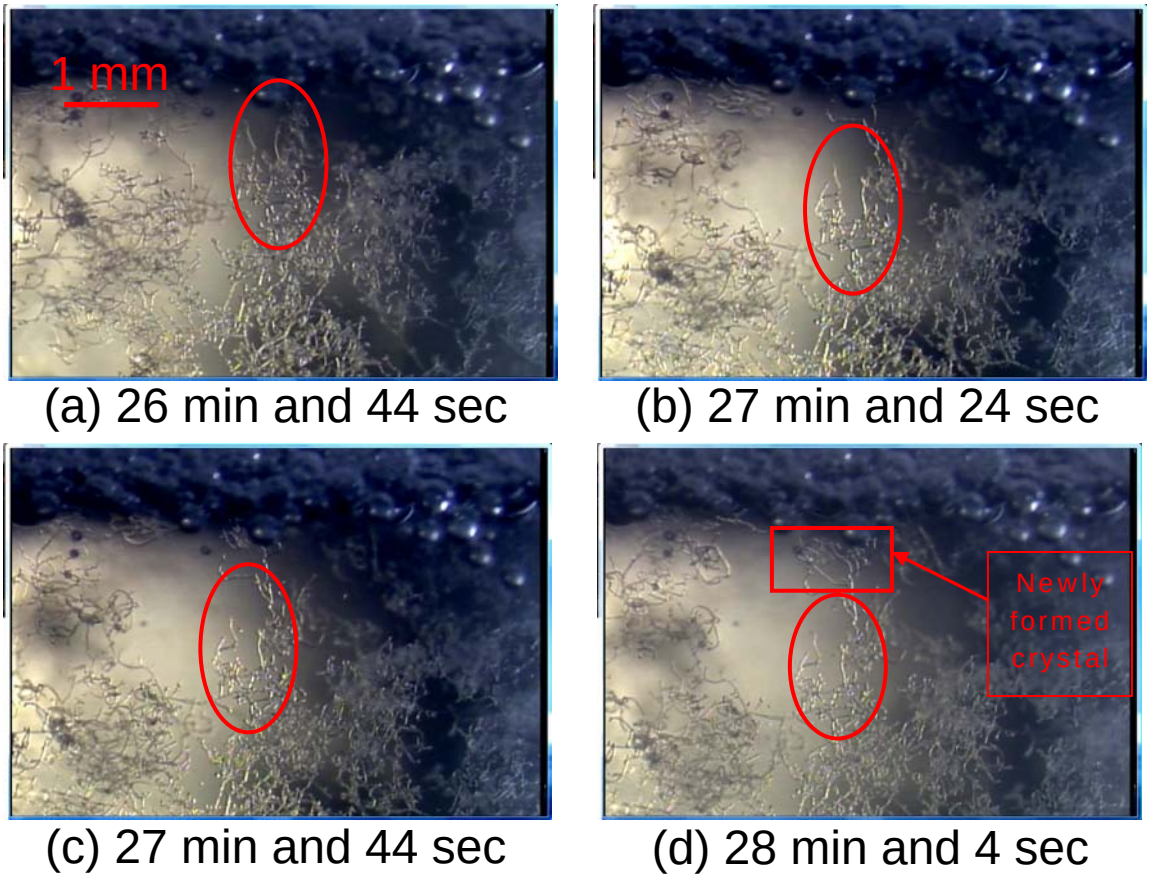


Figure 4.14: Growth of fibre-like crystals (Experiment C-1)

### 4.2.3 Mushy Hydrate Layer Growth Towards Bulk Water

As mentioned by Okutani et al. (2008), that the mechanism of the downward growth of "mushy" hydrate layer into the bulk water is unclear at present and closer observations are required to study the mechanism. Based on our observation using a microscope (Figure 4.15), the extent of the mushy hydrate layer in the bulk liquid solution increased due to the continuous hydrate formation on the base of the mushy hydrate layer (gas-liquid interface). There is also an animation given to illustrate how the mushy hydrate layer extends its length. Light blue triangle is an illustration of the mushy hydrate layer at 190 sec and the

dark blue color as the newly growth mushy hydrate layer at 10 sec after the light blue triangle.

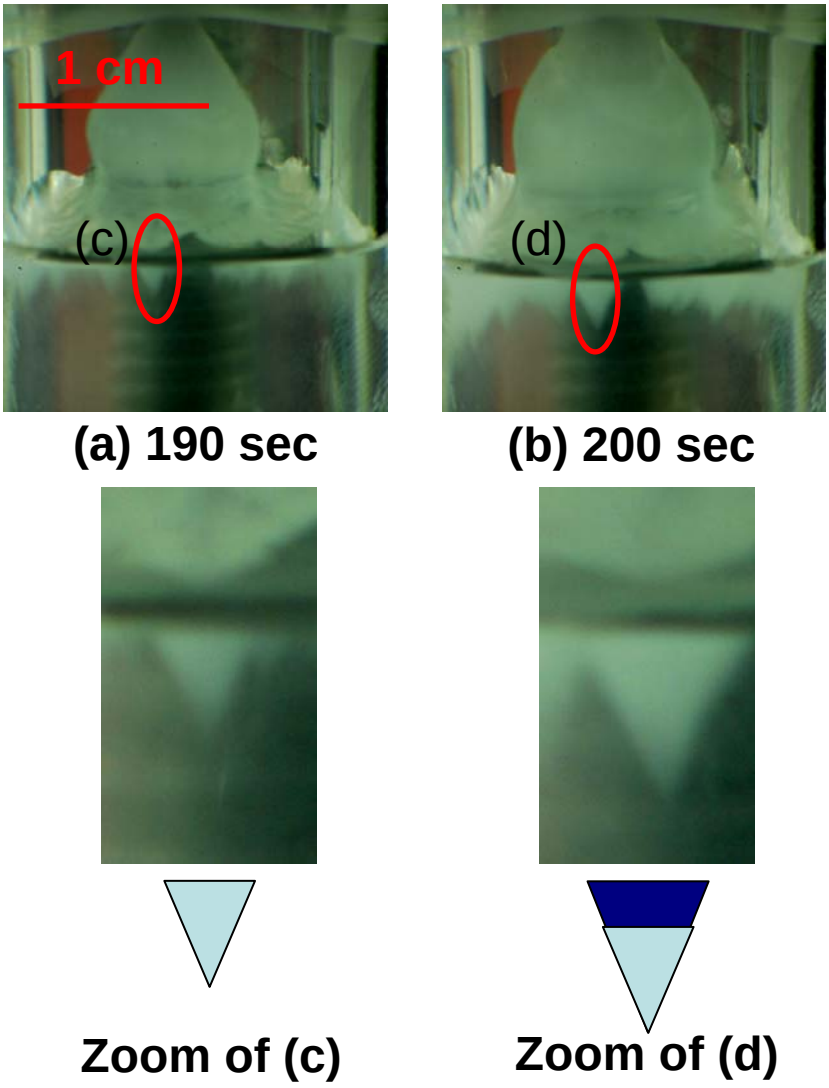


Figure 4.15: Mechanism of mushy hydrate growth (Experiment G-2)

The process of mushy hydrate layer growth towards the bulk water indicates that gas/water contact can be maintained through continuous water supply from the bulk to the interface. This requires that the mushy hydrate layer is porous so that the capillary mechanism enables water to travel through the pores from the bulk to the interface.

### 4.2.4 Hydrate Layer Growth on the Crystallizer Wall

Two types of hydrate crystals were also observed on the crystallizer wall (Figure 4.16). First on the right, it is crystals which look like a leaf which were seen to grow slowly (leaf-like crystal). On the other hand, a bulky hydrate was also seen attached to the wall which was found to grow faster that the leaf-like crystals.

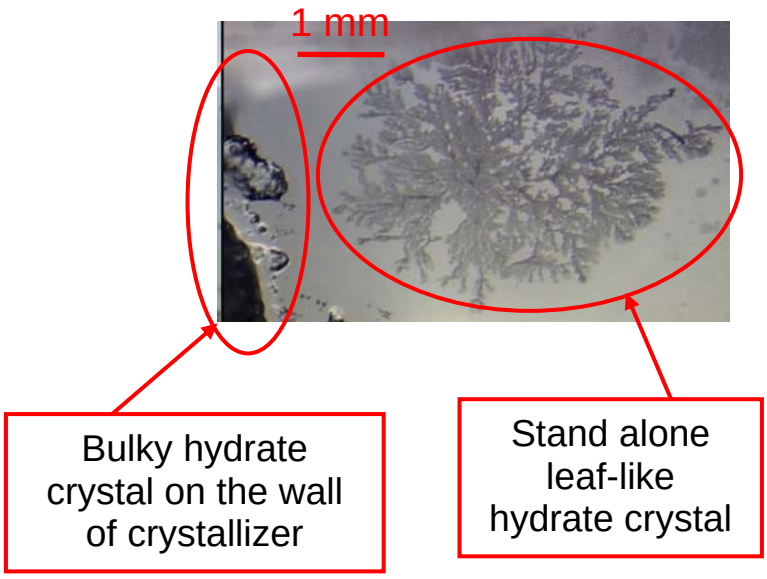


Figure 4.16: Two important objects discussed (Experiment G-3)

Once, the bulky hydrate layer touches the leaf-like hydrate, water is seen travelling inside the leaf-like crystal structure. This phenomenon is inferred from Figure 4.17 where the colour of the leaf-like crystal starts to change at the time when the bulky hydrate layer touches the leaf-like structure. At the same time the leaf-like hydrate crystal started to grow thicker possibly due to new water supply from the bulky hydrate layer. A less magnified view can be seen in the sequence of images in Figure 4.18.

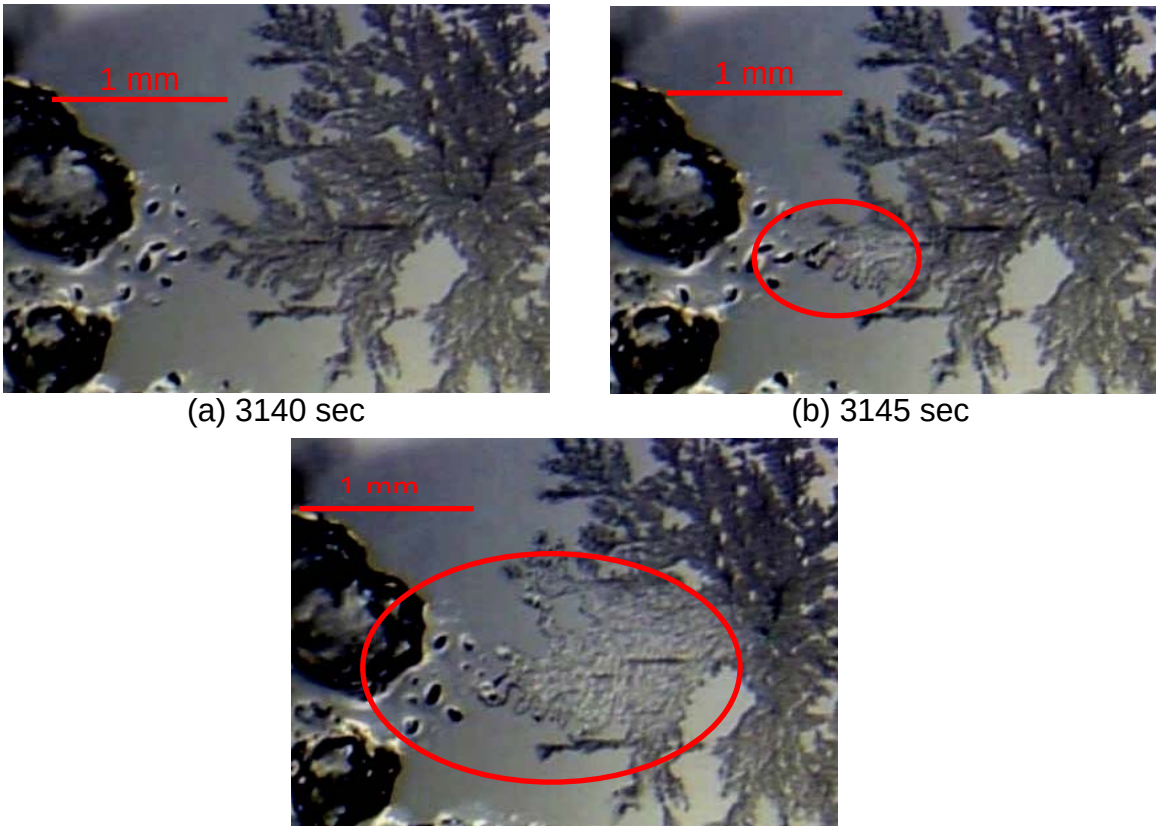


(a) 3140 sec (b) 3145 sec

(c) 3160 sec

Figure 4.17: Growth of leaf-like hydrate crystal at 13.1 degree of under-cooling

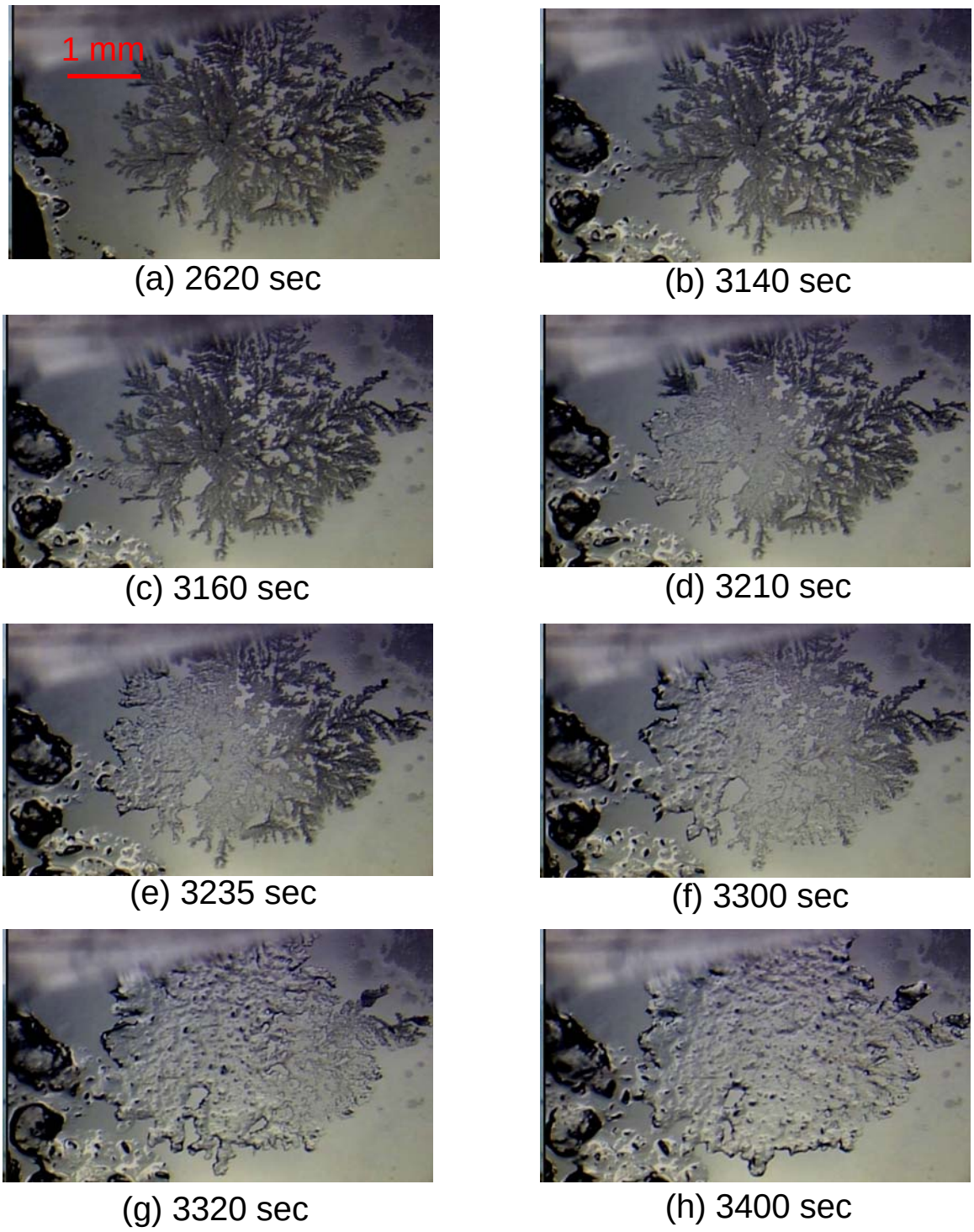


Figure 4.18: Less magnified view of leaf-like crystal growth (Experiment G-3)

### 4.2.5 Effect of Surfactant Concentration on the Morphology of Gas Hydrates

Three different surfactant concentrations were used. The concentrations are 2200ppm (high), 645ppm (medium), and 242ppm (low) and the surfactant type is Sodium Dodecyl Sulfate (SDS). SDS was chosen to compare to the other two because more literature data is available for this particular surfactant. These three different concentrations were chosen based on literature research on the effect of surfactant on the surface tension of water and the maximum water to hydrate conversion. According to Watanabe et al. (2005), 2200ppm concentration of SDS on water at ordinary ambient condition gives the critical concentration and according to W. Lin et al. (2004), 645 ppm is found to be the concentration that gives maximum storage capacity. Furthermore, 242ppm of SDS concentration is chosen because according to Zhong and Rogers that concentration gives a significant change in hydrate induction time. Many physical properties of liquid solutions, such as surface tension, are altered significantly when the surfactant concentration increases. Likewise, the hydrate formation rates are found to be affected by the concentration according to Zhong and Rogers (2000); Watanabe et al., 2005; Okutani et al., 2008.

In order to compare the morphology of three different surfactant concentration, the same experimental conditions were used. The experimental condition was P = 3200KPa, T=2.4$^{o}$C, and $\Delta$T=13.1$^{o}$C

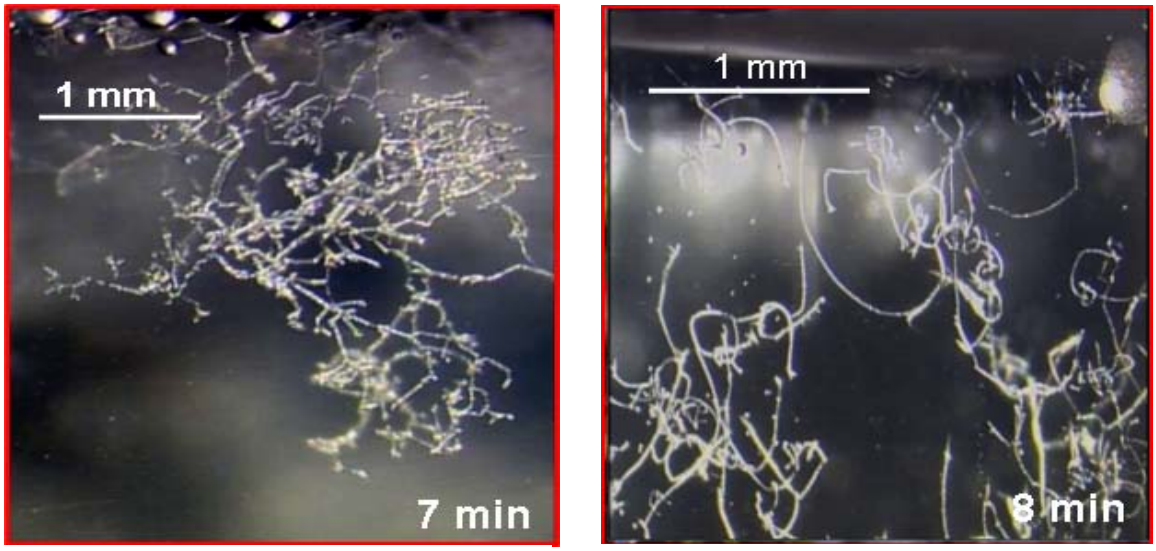


**(a)** **(b)**

Figure 4.19: Hydrate crystal growth at different surfactant concentrations (experiment B-1 and E-3). Surfactant concentration of 2200 ppm (a) and surfactant concentration of 645 ppm (b).

The morphology of hydrate crystal growth during both experiments showed similar patterns to the one discussed above, but as the concentration increased, the degree of branching increases as seen in Figure 4.19. The degree of branching at 242 ppm was found to be similar to that for the SDS-645 ppm experiment.

### 4.2.6 Effect of Under-cooling on the Morphology of Gas Hydrates

Three experiments with different degrees of under-cooling ($13.1^{o}$, $8^{o}$, and $3.6^{o}$) were conducted. SDS was used as the surfactant because it is the most widely known surfactant compared to the other two. The concentration used was 2200ppm. These three different degrees of subcooling were chosen because they are similar to those used by Lee et al.(2006), and Kumar et al. (2007) so that results can be compared. Figure 4.20 shows that

at high and medium degrees of under-cooling (Experiment B-1 and C-1), similar hydrate crystal growth was observed, but as the degree of under-cooling (ΔT) increases, the extent of hydrate crystal increases. At the lowest degree of under-cooling (Figure 4.20c), there is no significant hydrate crystal growth but a thin hydrate layer on the crystallizer wall can still be seen.

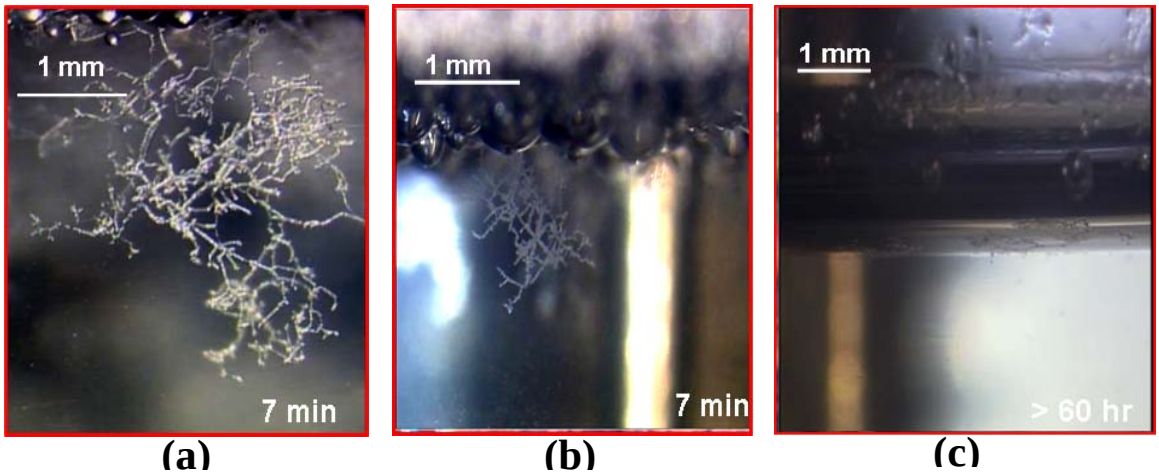


Figure 4.20: Hydrate crystal growth at different degree of under-cooling. ΔT =13.1°K (a), ΔT=8.0°K (b), and ΔT= 3.6°K (c).

## 4.3 Gas Uptake Measurement during Hydrate Formation

The moles of methane-propane gas consumed in the crystallizer due to hydrate formation are calculated by using the pressure and temperature data collected with the data acquisition system. In a closed system, like ours, the total number of moles in the system will remain constant at any given time. From this data, ratio of moles of gas consumed for hydrate formation in the systems with and without surfactant can be obtained. The ratio of moles of gas consumed for hydrate formation in the system with and without surfactant, ( $\frac{\Delta n_s}{\Delta n_w}$ ), can

be determined using the ratio of pressure drops ($P_{initial}$-P at time t) with and without surfactant ($\frac{\Delta P_s}{\Delta P_w}$) as shown in equation (1). $\Delta P_s$ and $\Delta P_w$ are the total pressure drops due to gas consumed during hydrate formation with and without surfactant present in the system, respectively.

$$\frac{\Delta n_s}{\Delta n_w} = \frac{\frac{\Delta P_s . V_s}{Z . R . T_s}}{\frac{\Delta P_w . V_w}{Z . R . T_w}} = \frac{\Delta P_s}{\Delta P_w} \qquad (1)$$

z is the compressibility factor calculated by Pitzer's correlation (Smith et al., 2001).

As shown in table 3.1 (experiment A-1 and B-1), Figure 4.21 and Figure 4.22, the ratio of pressure drop for system with and without SDS surfactant is 14.3 which indicate that when surfactant is present, 14.3 times more moles of gas consumed during hydrate formation compared to the system without additive.

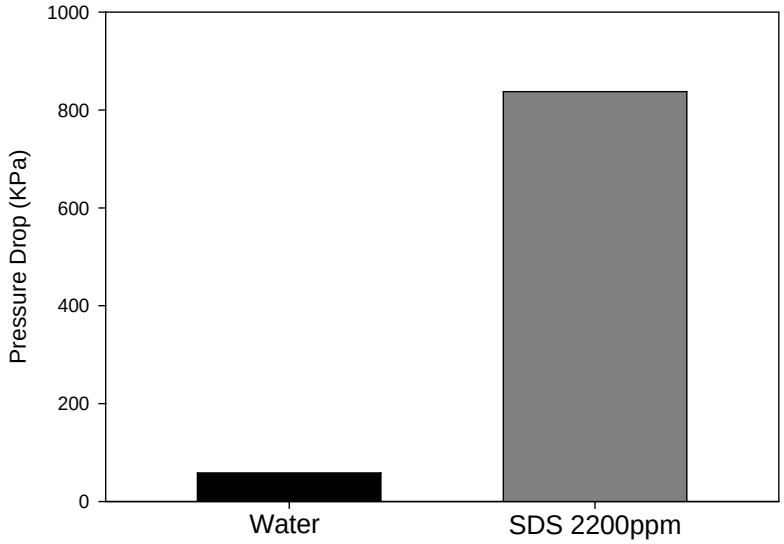


Figure 4.21: Final pressure drop comparison of system with and without surfactant with ΔT = 13.1 $^{o}$C. (Experiment A-1 and B-1)

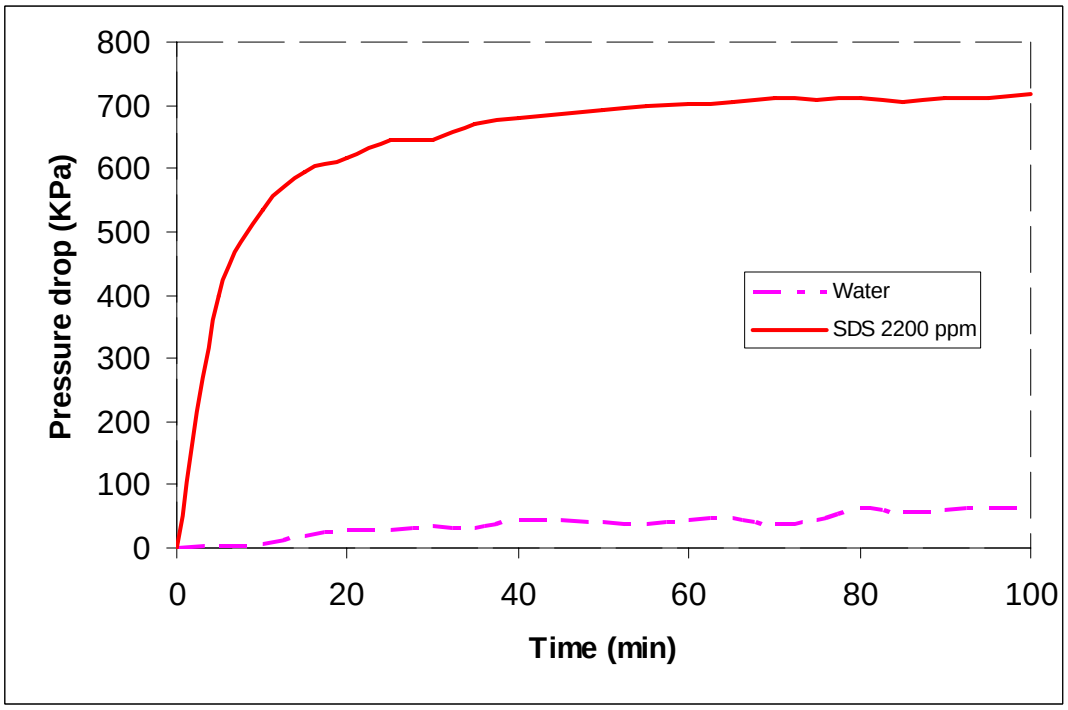


Figure 4.22: Pressure drop time evolution comparing system with and without surfactant (Experiment A-1 and B-1)

The increase observed in the uptake of gas when surfactant is present can be explained by considering the morphological observations during hydrate formation. For hydrate formation without any additives, hydrate will form at the gas-liquid interface as a thin rigid film and cover the gas-liquid interface. This phenomenon will limit or increase the barrier for gas to be adsorbed since gas must pass through the thin hydrate layer to find free water. However, when surfactant is present in the system, porous hydrate is believed to form at the interface of the gas-liquid which has the ability to renew the gas-liquid interface through capillary suction of water from the bulk liquid to the free surface. This phenomenon can be seen from the decrease of the liquid level due to its consumption during continuous hydrate formation along the crystallizer wall.

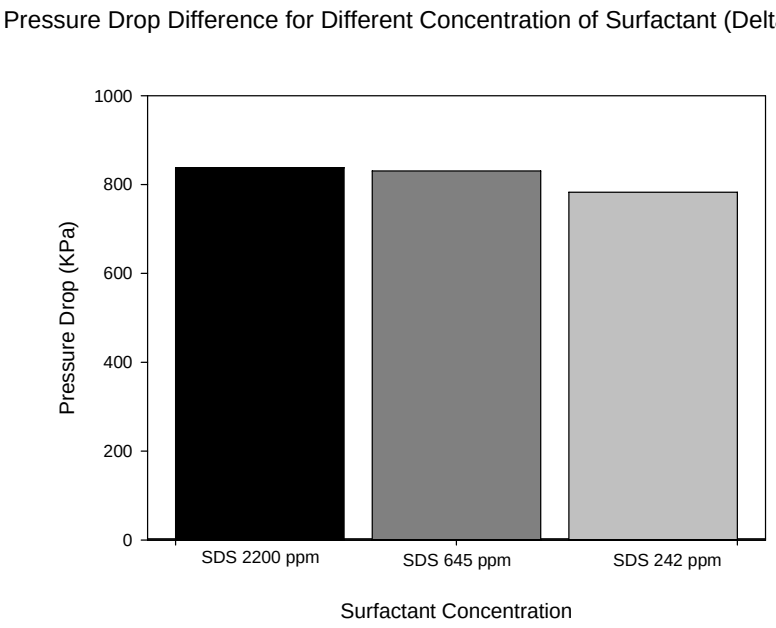


Figure 4.23: Final pressure drop comparison with different surfactant concentration with ΔT = 13.1 $^{o}$C (Experiment B-1,E-1, and F-1).

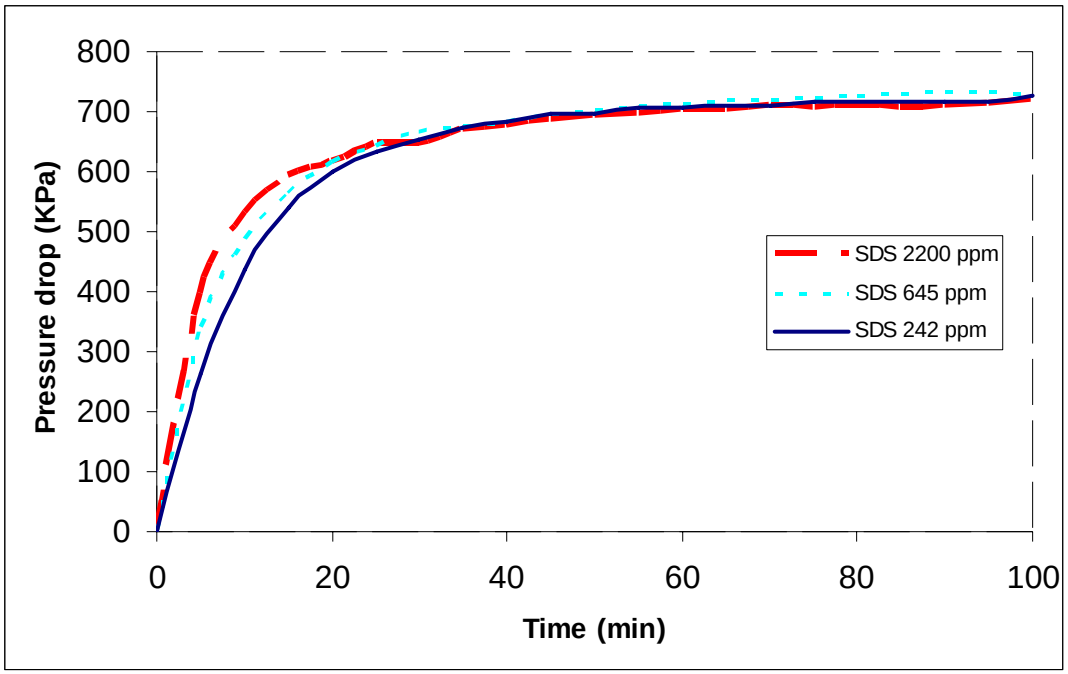


Figure 4.24: Pressure drop time evolution comparing system with three different surfactant concentrations

Experiments have also been conducted to compare the final pressure drop at different surfactant concentrations but at the same temperature and initial pressure. The results are summarized in Figure 4.23 and Figure 4.24. As seen, there is no significant difference in the total moles of gas consumed during hydrate formation which agree with results from Okutani et al (2008).

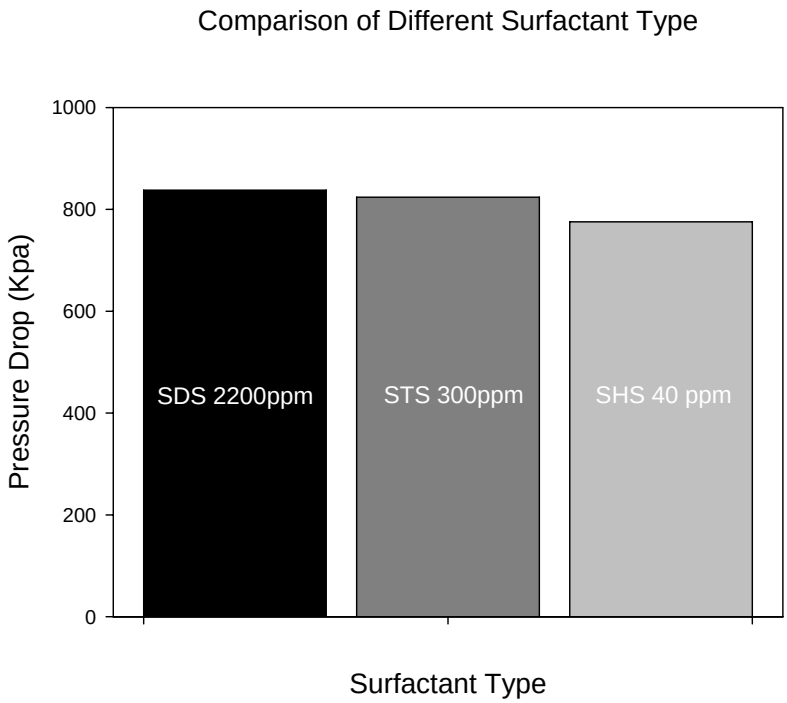


Figure 4.25: Final pressure drop comparison with different surfactant type with $\Delta T = 13.1^{o}C$ (Experiment B-1, G-1, and H-1).

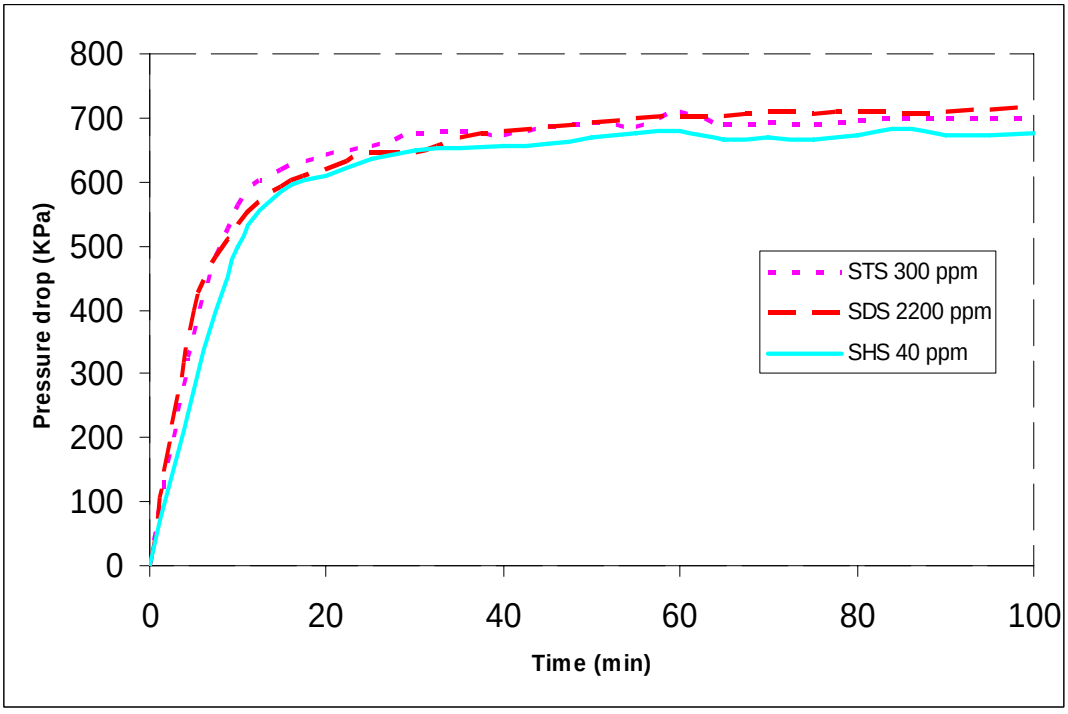


Figure 4.26: Pressure drop time evolution comparing system with three different surfactant types

Three other experiments have been done to compare the effect of surfactant type (SDS, STS, and SHS) on the gas uptake. All of the experiments were done at the same temperature and initial pressure. The results are summarized in Figure 4.25 and Figure 4.26. It is seen that there is no significant difference between SDS, STS and SHS. Finally, Table 4.5 shows a correlation between surface tension with the total pressure drop. It indicates that the lower the surface tension, more gas is being consumed for hydrate formation.

Table 4.5: Correlation between total pressure drop with surface tension

| | SDS-2200ppm | STS-300ppm | SHS-40ppm |
|---|---|---|---|
| Pressure Drop (Kpa) | 1006.6 | 992.8 | 937.7 |
| Surface Tension ($mN.m^{-1}$)[(a)] | ~ 30.9 | 39.4 | 50.3 |

(a) data was taken from Watanabe et al. (2005b)

## 4.4 Ice – Surfactant Interaction

In order to determine whether surfactant will attach to hydrate surface or not, this experiment which uses the ice surface to simulate a hydrate surface and the ice with known surface area is dipped into known concentration of SDS solution. As a result, the initial concentration of SDS solution can be compared with the final concentration after the ice being dipped into the solution.

It is known that surface tension of SDS solution decreases with increasing concentration up to a certain limit. Based on this information, a calibration curve of SDS concentration vs. contact angle (Figure 4.27) was made to measure the concentration of SDS solution.

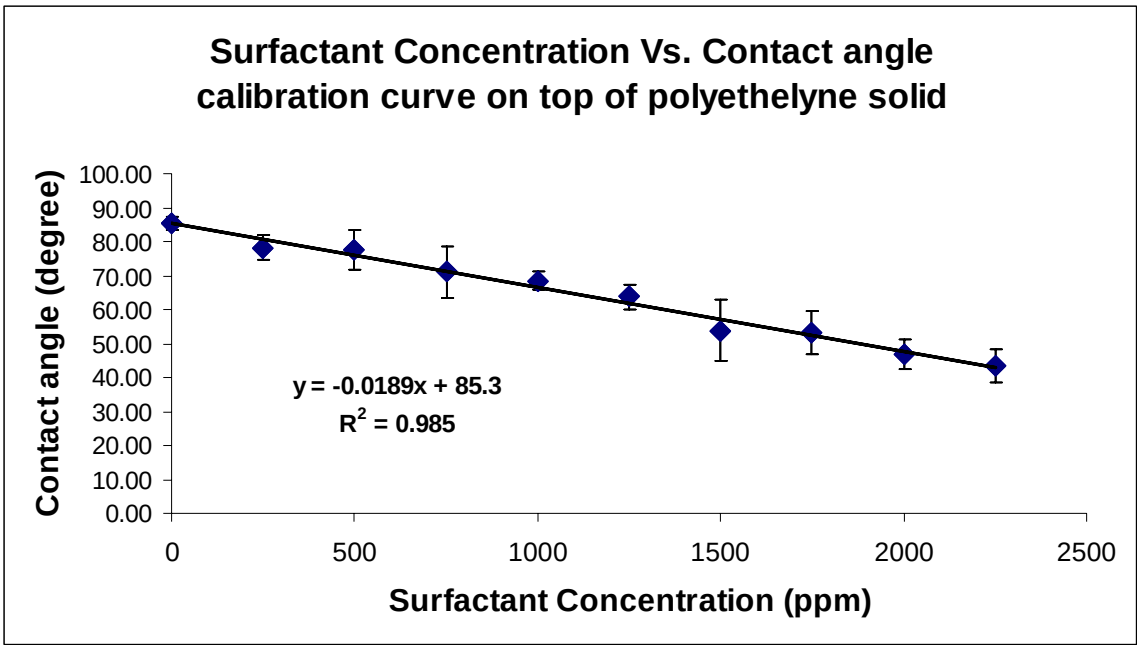


Figure 4.27: Calibration Curve of SDS range from 0 – 2250 ppm on top of Ultra High Molecular Weight Polyethylene surface

In this section, two experiments were done using two different initial concentration of SDS which are 1000 ppm and 2000 ppm. Half-sphere ice with a surface are ranging from 11.1 $cm^2$ to 11.7 $cm^2$ was also prepared. The contact angle measurements of initial SDS solution were shown in Table 4.6 and the contact angle measurements of final SDS solution and ice were shown in Table 4.7 for SDS 1000ppm, Table 4.8 for ice dipped in SDS 1000ppm solution, Table 4.9 for SDS 2000ppm, and Table 4.10 for ice dipped in SDS 2000ppm solution.

The results for both SDS 1000ppm and SDS 2000ppm show that there is an increase in contact angle which also means that surfactant concentration in the solution decreases. In other words it also indicates that some of the surfactant is attached to the surface of ice and it is true that the results from Table 4.8 and Table 4.10 indicated decrease in contact angle

which shows an increase in surfactant concentration. The changes in contact angle were more significant when the initial surfactant concentration is 2000ppm compared to 1000ppm.

Table 4.6: Pure component contact angle

| Exp. | Contact Angle |
|---|---|
| **Water** | 85.37 |
| **1000 ppm of SDS Solution** | 66.31 |
| **2000 ppm of SDS solution** | 46.34 |

Table 4.7: Contact angle of 10ml SDS solution after ice with surface area of 11.1 – 11.7 cm2 being dipped into the solution (Initial Concentration of SDS is 1000ppm)

| Exp. | Contact Angle |
|---|---|
| **SDS 1-A** | 66.73 |
| **SDS 1-B** | 67.82 |
| **SDS 1-C** | 66.50 |
| **SDS 1-D** | 65.49 |
| **SDS 1-E** | 66.24 |
| **Average** | 66.55 |
| **Stdev** | 0.85 |
| **median** | 66.50 |

Table 4.8: Contact angle of water from melted ice after being dipped into 1000ppm SDS solution

| Exp. | Contact Angle |
|---|---|
| **Ice 1-A** | 81.97 |
| **Ice 1-B** | 85.80 |
| **Ice 1-C** | 83.50 |
| **Ice 1-D** | 85.59 |
| **Ice 1-E** | 86.65 |
| **Average** | 84.70 |
| **Stdev** | 1.92 |
| **median** | 85.59 |

Table 4.9: Contact angle of 10ml SDS solution after ice with surface area of 11.1 – 11.7 $cm^2$ being dipped into the solution (Initial Concentration of SDS is 2000ppm)

| Exp. | Contact Angle |
|---|---|
| **SDS 2-A** | 48.19 |
| **SDS 2-B** | 49.53 |
| **SDS 2-C** | 49.76 |
| **SDS 2-D** | 47.02 |
| **SDS 2-E** | 46.86 |
| **Average** | 48.27 |
| **Stdev** | 1.36 |
| **median** | 48.19 |

Table 4.10: Contact angle of water from melted ice after being dipped into 2000ppm SDS solution

| Exp. | Contact Angle |
|---|---|
| **Ice 2-A** | 86.07 |
| **Ice 2-B** | 82.92 |
| **Ice 2-C** | 81.85 |
| **Ice 2-D** | 85.17 |
| **Ice 2-E** | 81.46 |
| **Average** | 83.49 |
| **Stdev** | 2.04 |
| **median** | 82.92 |

## 4.5 High Pressure Injection of Surfactant Solution

Figure 4.28 shows sequences of hydrate formation obtained from injecting 1ml of SDS solution into 24ml of $H_2O$ (Water) after the formation of a thin liquid film of the interface of the gas/liquid. The behavior of the macroscopic hydrate phase growth observed here is similar to the hydrate phase growth in the gas/water system (Lee et al., 2006). Bulky hydrate growth along the crystallizer wall was not seen if surfactant solution is injected after the formation of thin liquid film on the gas/liquid interface. Based on our observation for 48 min (Dynamic 1) and 2000 min (Dynamic 2), surfactant does not play a role as a promoter if the gas/liquid interface is already blocked by a thin film of hydrates. However, it is not

known how much time the surfactant needs to diffuse to the crystal surface. That aspect remains to be investigated.

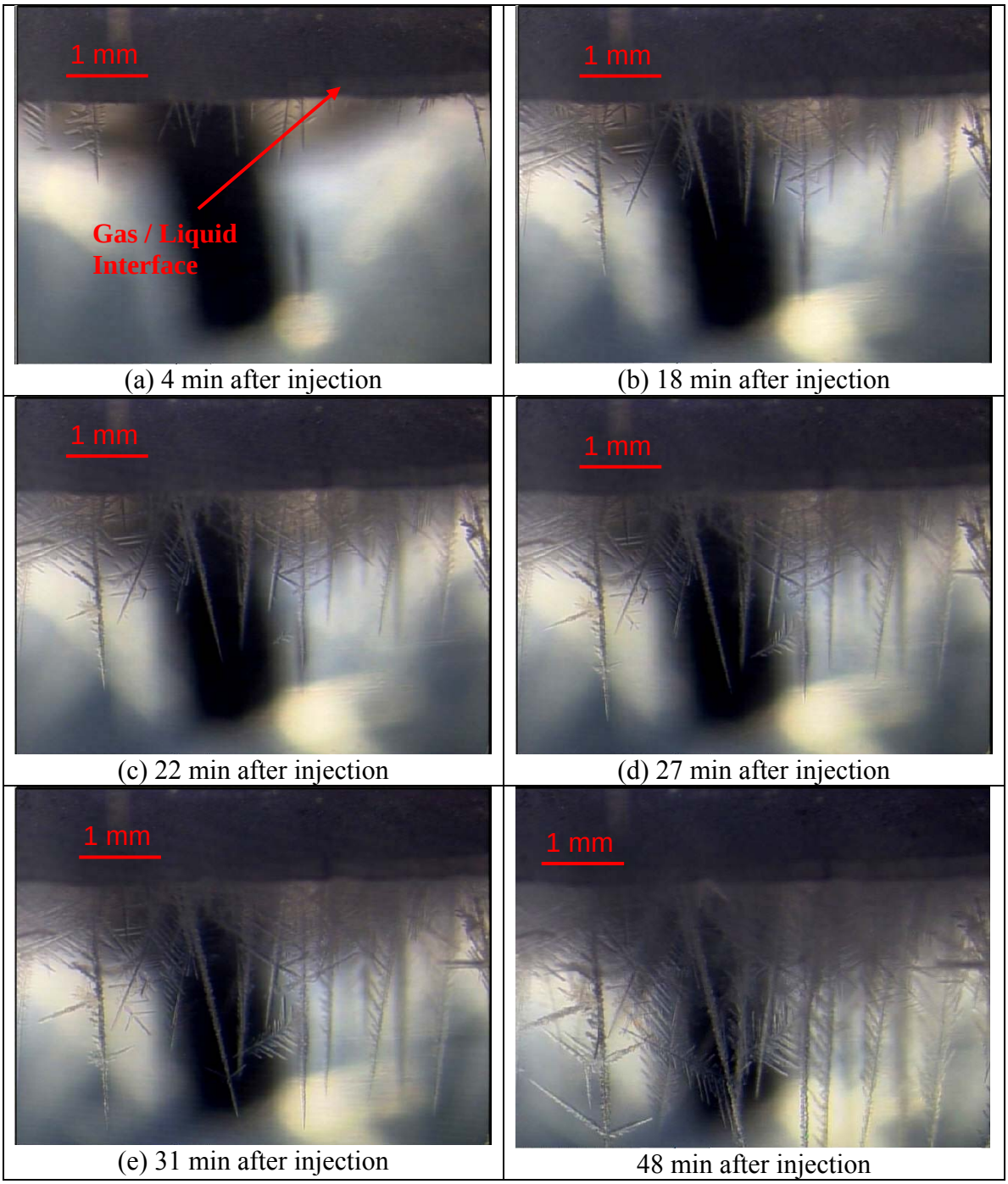


(a) 4 min after injection

(b) 18 min after injection

(c) 22 min after injection

(d) 27 min after injection

(e) 31 min after injection

48 min after injection

Figure 4.28: Typical sequences of hydrate phase growth at 13.1$^{o}$C of undercooling after SDS surfactant solution being injected after time 0 min (Time zero is not the induction time) (Experiment Dynamic 1)

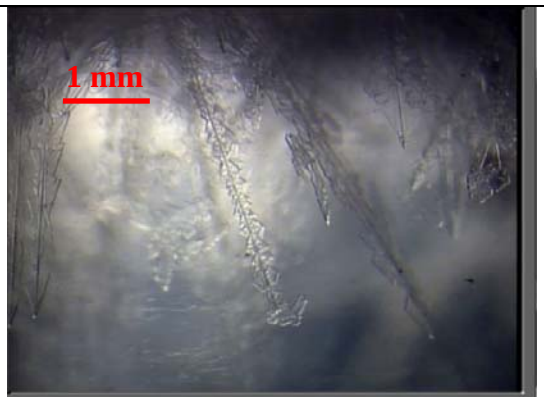


0 min after injection


100 min after injection


500 min after injection

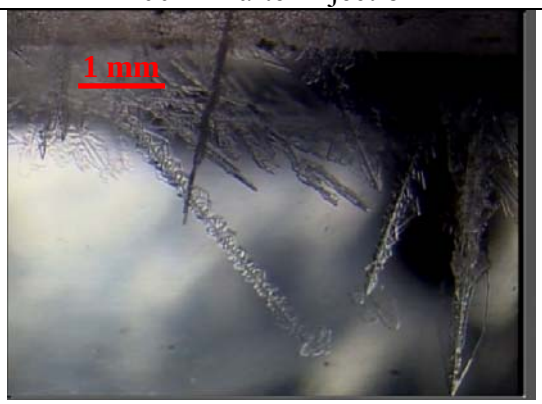


2000 min after injection

Figure 4.29: Typical sequences of hydrate phase growth at 13.1oC of undercooling after SDS surfactant solution being injected after time 0 min (Time zero is not the induction time) (Experiment Dynamic 2)

# Chapter 5: CONCLUSIONS AND RECOMMENDATIONS

## 5.1 Conclusions

The dynamics of methane-propane hydrate crystal growth in solution with or without the presence of surfactant (SDS, STS, and SHS) were studied. The surfactant concentrations used are 2200ppm, 645ppm, 242ppm for SDS, 300ppm for STS, and 40ppm for SHS. The conclusions are:

- When surfactant is present in the system, hydrate formation no longer started to form as thin solid film at the liquid-gas interface but started on the crystallizer walls (gas-solid-liquid line) and formed thick, bulky layers which grew upward (along the crystallizer wall above gas-liquid interface) and then, followed by radial growth along the gas liquid interface. This created a "mushy" hydrate layer that covered the gas-liquid interface and grew towards the bulk water.
- Unlike the system with pure water where needle-like dendritic crystals were found to grow from the gas-liquid interface to the bulk water, branches of fibre-like crystals were found to grow when surfactant is present in the system. It was also observed that increasing surfactant concentration increases branching of fibres compared to lower concentration.
- The degree of under-cooling affects the extent of hydrate formation where if $\Delta T$ increases, the extent of hydrate formation increases.

- In addition, the presence of 2200ppm of SDS surfactant in the liquid phase also promotes hydrate growth in the system and increases the moles of gas consumed by 14.3 -18.7 times compared to the system without surfactant under the same experimental conditions. This increase is related to the change in hydrate morphology whereby a more porous hydrate forms with enhanced water/gas contacts.
- Finally, contact angle measurements were done with ice and surfactant solutions whereby it was found that surfactants adsorb on the ice surface.

## 5.2 Recommendations

- Study the morphology of Gemini surfactant (surfactant molecule possessing more than one hydrophobic tail and hydrophilic head group) and green surfactant (surfactant which is proven to be environmental friendly)
- Surfactant alkyl chain length studied in this work involved C12, C14 and C16. A wider study incorporating shorter carbon length up to C4 should be studied to investigate any possible effects this would have on the morphology of hydrate formation.
- For surfactant addition to be considered a valid alternative to the existing technologies for natural gas hydrate storage and transport, process scale up and detailed economic analysis of the process should be carried out. This will facilitate a cost comparison between the surfactant system process and other available technologies.
- Measure contact angle changes when surfactant is present in the system on top of stainless steel surface.

# REFERENCES


Aaron, D., and Tsouris, C., **2005**. *Separation Science and Technology.* 40(1-3), 321-348.

Daimaru, T., Yamasaki, A., and Yanagisawa, Y., **2007**. *Natural Gas Hydrate / Clathrate.* 56(1-3), 89-96.

Davidson, D. W., **1973**. *Gas Hydrates*, Plenum Press, New York.

Davy, H., **1811**. *Phil Trans Roy Soc (London).* 101, 1-35.

Dholabhai, P. D. K., N.; Bishnoi, P.R., **1992**. Annual Meeting of the Petroleum Society of CIM., Calgary, Alberta,June 7-10.

Di Profio, P., Arca, S., Germani, R., and Savelli, G., **2005**. *Chemical Engineering Science.* 60(15), 4141-4145.

Di Profio, P., Arca, S., Germani, R., and Savelli, G., **2007**. *Journal of Fuel Cell Science and Technology.* 4(1), 49-55.

Eick, R. M., and Klara, S. M., **1990**. *Chem.Eng.Comm.* 90, 23-33.

Englezos, P., **1993a**. *I&EC Research.* 32, 1251-1274.

Englezos, P., Kalogerakis, N., Dholabhai, P. D., and Bishnoi, P. R., **1987a**. *Chem. Eng. Sci.* 42(11), 2647.

Englezos, P., Kalogerakis, N., Dholabhai, P. D., and Bishnoi, P. R., **1987b**. *Chem. Eng. Sci.* 42(11), 2659.

Englezos, P., and Lee, J. D., **2005**. *Korean Journal of Chemical Engineering.* 22(5), 671-681.

Englezos, P. H., S. G., **1993b**. *The Stability of Permafrost and Gas Hydrates Subject to Global Warming.* Proc. Third (1993) International Offshore and Polar Engineering Conference, Singapore,June.

Fu, B., **2002**. *The development of advanced kinetic hydrate inhibitors*, Royal Society of Chemistry, Cambridge, UK.

Gayet, P., Dicharry, C., Marion, G., Graciaa, A., Lachaise, J., and Nesterov, A., **2005**. *Chemical Engineering Science.* 60(21), 5751-5758.

Gudmundsson, J. S., Andersson, V., Levik, O.I. , and Mork, M., **1999**. *Hydrate Technology for Capturing Stranded Gas.* 3rd International Conference on Gas Hydrates, Salt Lake City,July 18-22.

Gudmundsson, J. S., Andersson, V., Levik, O.I., Parlaktuna, M., **1998**. *Hydrate Concept for Capturing Associated Gas*. EUROPEC, The Hague, The Netherlands,20-22 October.

Gudmundsson, J. S., Graff, O F., **2003**. *Hydrate Non-Pipeline Technology for Transport of Natural Gas*. 22nd World Gas Conference, Tokyo, Japan,June 1-5.

Gudmundsson, J. S., Mork, M., and Graff, O. F., **2002**. *Proc. 4th International Conference on Gas Hydrates, Yokohama May 19-23, 2002.* 997-1002.

Hammerschmidt, E. G., **1934**. *Industrial and Engineering Chemistry.* 26, No. 8, 851-855.

Hansen, A. B. C., T.L.; Bass, R.M., **1999**. Proceedings of the Annual Offshore Technology Conference691-701.

Herri, J., Gruy, F., and Cournil, M., **1996**. *International Conference on Natural Gas Hydrates, 2nd, Toulouse,June 2-6, 1996.* 243-250.

Huo, Z., Freer, E., Lamar, M., Sannigrahi, B., Knauss, D. M., and Sloan, E. D., **2001**. *Chemical Engineering Science.* 56(17), 4979-4991.

Ivanhoe, L. F., **1993**. *Oil & Gas Journal.* 91(2), 87-91.

Kalogerakis, N., Jamaluddin, A. K. M., Dholabhai, P. D., and Bishnoi, P. R., **1993**. *SPE Intnl. Symp. on Oilfield Chemistry, New Orleans 3/2-5/93.* SPE25188, 375.

Kang, S. P., and Lee, H., **2000**. *Environmental Science & Technology.* 34(20), 4397-4400.

Karaaslan, U., and Parlaktuna, M., **2000**. *Energy & Fuels.* 14(5), 1103-1107.

Karaaslan, U., Uluneye, E., and Parlaktuna, M., **2002**. *Journal of petroleum science engineering.* 35(1), 49.

Katz, D. L. C. D. K. R. P., F. H.; Vary J. A.; Elenbaas, J.R.; Weinaug, C. F., **1959**. *Handbook of Natural Gas Engineering*, McGraw Hill, New York

Katz, D. L. L., R.L., **1991**. *Handbook of Natural Gas Engineering 2nd ed.*, McGraw Hill, New York.

Klein Nagelvoort, R., **2000**. *Large-Scale GTL – A Commercially Attractive Alternative to LNG*. Natural Gas Technology Workshop, Norwegian University of Science and Technology, Trondheim,November 28-29.

Knox, W. G., Hess, M., Jones, G. E., and Smith, H. B., **1961**. *Chem. Eng. Prog.* 57(2), 66 - 71.

Koh, C. A., **2002**. *Chemical Society Reviews.* 31(3), 157-167.

Kumar, R., Lee, J. D., Song, M., and Englezos, P., **2007**. *Journal of Crystal Growth.* 310, 1154-1166.

Kumar, R., Linga, P., Moudrakovski, I., Ripmeester, J. A., and Englezos, P., **2008**. *American Institute of Chemical Engineers.* 54(8), 2132-2144.

Kutergin, O. B., Melnikov, V. P., and Nesterov, A. N., **1992**. *Reports of the Russian Academy of Sciences.* 323(N3), 349.

Kvenvolden, K. A., **1988**. *Chemical Geology.* 71(1/3), 41.

Lee, J. D., Song, M., Susilo, R., and Englezos, P., **2006**. *Crystal growth design.* 6(6), 1428.

Lin, W., Chen, G. J., Sun, C. Y., Guo, X. Q., Wu, Z. K., Liang, M. Y., Chen, L. T., and Yang, L. Y., **2004**. *Chemical Engineering Science.* 59(21), 4449-4455.

Linga, P., Adeyemo, A., and Englezos, P., **2008**. *Environmental Science & Technology.* 42(1), 315-320.

Linga, P., Kumar, R. N., and Englezos, P., **2007**. *Chemical Engineering Science.* 62(16), 4268-4276.

Link, D. D., Ladner, E. P., Elsen, H. A., and Taylor, C. E., **2003**. *Fluid Phase Equilibria.* 211(1), 1-10.

Lovell, D. P., M., **2003**. *Journal of Petroleum Technology* 55, 65-68.

Makogon, Y. F., and Tsarev, V. I. C. N. V., **1972**. *Doklady Akademii Nauk SSSR.* 205, 700-703.

Makogon, Y. F., Holditch, S. A., and Makogon, T. Y., **2007**. *Journal of Petroleum Science and Engineering.* 56(1-3), 14-31

Mehta, A. P. H., P.B.; Cadena, E.R.; Weatherman, J.P., **2002**. Proceedings of the Annual Offshore Technology Conference SPE565-571.

Mel'nikov, P., Nesterov, A. N., and Feklistov, V. V., **1998**. *Khimiia v Interesakh Ustoichivogo Razvitiia.* 6, 97-102.

Metz, B., O. Davidson, H. C. de Coninck, M. Loos, and L. A. Meyer (eds.). **2005**. "*IPCC Special Report on Carbon Dioxide Capture and Storage. Prepared by Working Group III of the Intergovernmental Panel on Climate Change* ", Cambridge, United Kingdom and New York, NY, USA.

Mori, Y., & Mochizuki, T., **1996**. *Modeling of mass transport across a hydrate layer intervening between liquid water and guest fluid phases.* Second international symposium on gas hydrates,, Toulousepp. 267-274.

Mori, Y. H., **2003**. *J Chem Ind Eng.* 54, 1-17.

Narita, H., and Uchida, T., **1996**. *International Conference on Natural Gas Hydrates, 2nd, Toulouse,June 2-6, 1996.* 191-197.

Ngan, Y. T., and Englezos, P., **1996**. *Ind. Eng. Chem. Res.* 35, 1894-1900.

Ohmura, R., Matsuda, S., Uchida, T., Ebinuma, T., and Narita, H., **2005**. *Crystal Growth & Design.* 5(3), 953-957.

Ohmura, R., Shimada, W., Uchida, T., Mori, Y. H., Takeya, S., Nagao, J., Minagawa, H., Ebinuma, T., and Naritay, H., **2004**. *Philosophical Magazine.* 84(1), 1-16.

Okutani, K., Kuwabara, Y., and Mori, Y. H., **2008**. *Chemical Engineering Science.* 63(1), 183-194.

Ripmeester, J., and Ratcliffe, C., **1999**. *Journal of Structural Chemistry.* 40, 654.

Ripmeester, J. A., and Ratcliffe, C. I., **1988a**. *J. Phys. Chem.* 92(2), 337-9.

Ripmeester, J. A., Tse, J. S., Ratcliffe, C. I., and Powell, B. M., **1987**. *Nature.* 325, 135-136.

Rogers, R. E., Zhong, Y., Etherridge, J. A., Arunkumar, R., Pearson, L. E., and Hogancamo, T. K., **2005**. *Micellar gas hydrate stroage process*. Fifth International Conference on Gas Hydrates, Trondhei, Norway1361-1365.

Sloan, E. D., **1990**. *Marcel-Dekker, Inc, New York.* 664.

Sloan, E. D., **2003**. *Nature.* 426(6964), 353-359.

Sloan, E. D. J., **1998**. *Clathrate Hydrates of Natural Gasses*, Marcel Dekker, New York.

Smith, J. M., Van Ness, H. C., and Abbott, M. M., **2001**. *Introduction to Chemical Engineering Thermodynamics*, Macgraw-Hill, Inc., New York.

Sun, Z.-g., Wang, R., Ma, R., Guo, K., and Fan, S., **2003a**. *Energy Conversion and Management.* 44(17), 2733-2742.

Sun, Z., Wang, R., Ma, R., Guo, K., and Fan, S., **2003b**. *International journal of energy research.* 27(8), 747.

Susilo, R., Moudrakovski, I. L., Ripmeester, J. A., and Englezos, P., **2006**. *Journal of Physical Chemistry B.* 110(51), 25803-25809.

Susilo, R., Ripmeester, J. A., and Englezos, P., **2007**. *Chemical Engineering Science.* 62(15), 3930-3939.

Taylor, M. a. F., A. **2001**. *The BG Hydrate Project – Technology Development*. AIChE Spring National Meeting.

Tulk, C., Ripmeester, J., and Klug, D., **2000**. *Gas hydrates, challenges for the future.* NYAS 912, 859.

Uchida, T., Moriwaki, M., Takeya, S., Ikeda, I. Y., Ohmura, R., Nagao, J., Minagawa, H., Ebinuma, T., Narita, H., Gohara, K., and Mae, S., **2004**. *Aiche Journal.* 50(2), 518-523.

van der Waals, J. H., and Platteeuw, J. C., **1959**. *Nature.* 183, 4659, 462.

Voormeij, D. A., and Simandl, G. J., **2004**. *Geoscience Canada.* 31(1), 11-22.

Vysniauskas, A., and Bishnoi, P. R., **1983**. *Chemical Engineering Science.* 38(7), 1061-1072.

Watanabe, K., Imai, S., and Mori, Y. H., **2005a**. *Chemical engineering science.* 60(17), 4846-4857.

Watanabe, K., Niwa, S., and Mori, Y. H., **2005b**. *Journal of Chemical & Engineering Data.* 50(5), 1672-1676.

WEO, W. E. O., **2007**. *China and India Insights*, International Energy Agency.

Zeng, H., Moudrakovski, I. L., Ripmeester, J. A., and Walker, V. K., **2006a**. *Aiche Journal.* 52(9), 3304-3309.

Zeng, H., Walker, V. K., and Ripmeester, J. A., **2007**. *Angewandte Chemie-International Edition.* 46(28), 5402-5404.

Zeng, H., Walker, V.K. and J.A. Ripmeester. **2005**. *Examining The Classification of Low Dosage Hydrate Inhibitors*. Proc 5th International Conference on Gas Hydrate, Norway,June 12-16, 1295-1299.

Zeng, H., Wilson, L. D., Walker, V. K., and Ripmeester, J. A., **2003**. *Canadian Journal of Physics.* 81(1-2), 17-24.

Zeng, H., Wilson, L. D., Walker, V. K., and Ripmeester, J. A., **2006b**. *Journal of the American Chemical Society.* 128(9), 2844-2850.

Zhang, J. S., Lee, S., and Lee, J. W., **2007**. *Journal of Colloid and Interface Science.* 315(1), 313-318.

Zhong, Y., and Rogers, R. E., **2000**. *Chemical Engineering Science.* 55(19), 4175-4187.